# An Innovative Approach to Determination of Double-Porosity Fractured Aquifers Hydraulic Parameters Using Artificial Neural Network

**Tahereh Azari**
Shiraz University
**Mahmoud Mohammad Rezapour Tabari** ( mrtabari57@gmail.com )
University of Mazandaran https://orcid.org/0000-0002-4837-5026

**Research Article**

**Keywords:** Aquifer parameters, Double porosity, Well function, Artificial neural networks, Principal component analysis (PCA)

**Posted Date:** June 9th, 2021

**DOI:** https://doi.org/10.21203/rs.3.rs-587986/v1

# An Innovative Approach to Determination of Double-Porosity Fractured Aquifers Hydraulic Parameters Using Artificial Neural Network

Tahereh Azari[1], Mahmoud Mohammad Rezapour Tabari[2]

[1]Department of Earth Sciences, College of Sciences, Shiraz University, Shiraz 7136713565, Iran, E-mail: azari.azadeh3420@gmail.com

[2]Associate Prof., Department of Civil Engineering, Faculty of Engineering and Technology, University of Mazandaran, Babolsar, Iran, E-mail: mrtabari@umz.ac.ir (Corresponding Author)

[2]Center of Excellence in Risk Management and Natural Hazards, Isfahan University and Technology, Isfahan, Iran

## Abstract

Accurate determination of hydraulic parameter values is the first step to the sustainable development of an aquifer. Since Theis (1935), type curve matching technique (TCMT) has been used to estimate the aquifer parameters from pumping test data. The TCMT is subjected to graphical error. To eliminate the error an Artificial Neural Network (ANN) is developed as an alternative to the conventional TCMT by modeling the Bourdet-Gringaten's well function for the determination of the fractured double porosity aquifer parameters. The neural network model is developed in a six-step protocol based on multi-layer perceptron (MLP) networks architecture and is trained for the well function of double porosity aquifers by the back propagation method and the Levenberg-Marquardt optimization algorithm. By applying the principal component analysis on the training input data and through a trial-and-error procedure the optimum structure of the network is fixed with the topology of [3×6×3]. The replicative, predictive and structural validity of the developed network are evaluated with synthetic and real field data. The developed network

provides an automatic and fast procedure for the double porosity aquifer parameter determination that eliminates graphical errors inherent in the conventional TCMT. The network receives pumping test data and provides the user with the aquifer parameter values.

**Keywords:** Aquifer parameters; Double porosity; Well function; Artificial neural networks; Principal component analysis (PCA).

## 1 Introduction

The aquifer parameters obtained by the type-curve graphical method are rather subjective due to graphical and personal errors and the accurate results are usually not obtained. In spite of a multitude of papers published on the ANN application in water resources, published works on aquifer parameters estimation are very limited. In recent years, some suitable approaches based on artificial neural networks (ANNs) have been developed as an alternative approach to model the well functions and remove the errors resulted from graphical type curve matching techniques. Lin and Chen (2005) proposed an ANN approach to estimate aquifer parameters of leaky confined aquifers based on a combination of a Radial Basis Function Network (RBFN) and Hantush and Jacob (1995) analytical solution. Lin and Chen (2006) also suggested the combination of an ANN and the Theis (1935) analytical solution in confined aquifers. The problem with Lin and Chen networks is that as the number of time-drawdown data increases, the dimensionality of networks becomes larger and they also have to be trained and tested for each individual set of pumping test data (Samani et al. 2007). Accordingly, Samani et al. (2007) proposed simple ANN by replacing the gradient descent algorithm with the faster Levenberg-Marquardt (LM) training algorithm and applying Principal Component Analysis (PCA) on the training data set to estimate confined aquifer parameters without the aforementioned limitations. Later Lin et al. (2010) applied the PCA on the

training and testing data patterns in the development of an ANN for the parameter estimation of anisotropic aquifers. Later Azari et al. (2015) proposed two ANN models for the determination of leaky confined aquifer with and without storage in the aquitard. Azari and Samani (2018) developed an ANN for modeling the Neuman's well function to estimate the parameters of unconfined aquifers. Cahyadi et al. (2021) developed an artificial neural network back propagation (ANNBP) model based on the rock quality designation, lithology permeability index, depth index, and gouge content designation parameters in order to prediction the distribution of K value isotopically for groundwater modeling. Recently, Tabari et al. (2021) proposed a SCMTA model for the determination of confined aquifers parameters as an alternative to the type-curve graphical method and the existing ANN approaches.

As mentioned, existing researches have focused on estimating the effective parameters of aquifers with homogeneous conditions by ANN approaches; however, aquifers are usually heterogeneous and anisotropic in real situations. The double-porosity fractured aquifers are an example of aquifers with heterogeneous conditions. To the best of our knowledge, no artificial intelligence (AI) model has been used to determine the effective parameters of double-porosity fractured aquifers with heterogeneous conditions.

Hydrogeological parameters such as transmissibility and storage coefficient are not clear-cut and most of the time they are associated with uncertainties. Among different AI techniques, in this study, a simple ANN model has been proposed to investigate the feasibility of acquiring hydrological parameters for double-porosity fractured aquifers with heterogeneous conditions.

The ANN receives the pumping test data as inputs and derives the optimal match points as outputs to determine the double-porosity fractured aquifer parameters with heterogeneous conditions. Synthetic data and in situ field data have been adopted to test the applicability and reliability of

71 the proposed methodology. Finally, the performance of the proposed model in generating the
72 match-point coordinates is compared with TCMT.
73 Therefore, the objective of this study is to develop an alternative approach and model the Bourdet-
74 Gringarten's well function (Eq. (5)) for estimation of the double-porosity fractured aquifers
75 parameters and remove the errors resulted from graphical type curve matching techniques. The
76 developed model is recommended as an efficient and accurate tool to the type-curve graphical
77 method for the determination of parameter values of double porosity aquifers.
78

79 **2 Double porosity fractured aquifer well function**

80 Based on the double porosity concept, initially introduced by Barenblatt et al. (1960), Bourdet and
81 Gringarten (1980) developed an analytical model for the determination of hydraulic properties of
82 fractured aquifers. The double porosity concept assumes the existence of two porous regions of
83 distinctly different properties within the aquifer. The fractures with a high conductivity and low
84 storage capacity which transmit water to the well and the matrix blocks region with a low
85 conductivity and high storage capacity which feed water only to the fractures. The concept of the
86 double porosity flow was also used by Warren and Root (1963), Kazemi et al. (1969), Boulton and
87 Streltsova (1977), Moench (1984), and Sen (1988). In the Bourdet-Gringarten model the
88 homogeneous and isotropic matrix blocks are separated from each other either by an orthogonal
89 system of continuous uniform fractures or by equally spaced horizontal fractures. The pressure
90 difference between fractures and matrix blocks which causes the flow of water from the blocks
91 into the fractures, known as inter-porosity flow, is under a pseudo-steady state condition. The flow
92 through the fractures to the well is radial and in an unsteady state condition. When a pumping well
93 fully penetrates a fracture and is pumped at a constant rate in a fractured confined aquifer,

dewatering occurs and creates a cone of depression in the piezometric surface (Fig. 1). Bourdet and Gringarten (1980) state that in a fractured aquifer of the double porosity type the drawdown response to pumping as observed in observation wells can be expressed as:

$$s = \frac{Q}{4\pi T_{\mathrm{f}}} \mathrm{F}(u^*,\ \lambda, \omega) \tag{1}$$

$$u^* = \frac{T_{\mathrm{f}}\, t}{(S_{\mathrm{f}} + \beta S_{\mathrm{m}}) r^2} \tag{2}$$

$$\lambda = \alpha\, r^2 \frac{K_{\mathrm{m}}}{K_{\mathrm{f}}} \tag{3}$$

$$\omega = \frac{S_{\mathrm{f}}}{S_{\mathrm{f}} + \beta S_{\mathrm{m}}} \tag{4}$$

$$\mathrm{F}(u^*, \lambda, \omega) = 2.3 \log(2.25u^*) + \mathrm{Ei}\left(-\frac{\lambda u^*}{\omega(1-\omega)}\right) - \mathrm{Ei}\left(-\frac{\lambda u^*}{(1-\omega)}\right) \tag{5}$$

$$\mathrm{Ei}(-\mathrm{x}) = -\int_0^{\mathrm{x}} \frac{\mathrm{e}^{-\mathrm{u}}}{\mathrm{u}}\, \mathrm{du} \tag{6}$$

$$\alpha = 4n(n+2)/l^2 \tag{7}$$

where, $s$ $[L]$ is the drawdown measured at time $t$ [T] in an observation well located at the distance $r$ [L] from the pumping well, $Q$ is constant discharge rate of pumped well [$L^3T^{-1}$], $T$ [$L^2T^{-1}$] is transmissibility, $S$ is storativity, $K$ [$LT^{-1}$] is hydraulic conductivity, $\lambda$ is the inter-porosity flow coefficient, $\omega$ is the ratio of the storativity of the fissure system to that of the total reservoir (fissures + matrix blocks), $u$ is an argument known as dimensionless time, $\alpha$ is shape factor (parameter characteristic of the geometry of the fractures and matrix blocks) and $\beta$ is a factor, for early-time analysis it equals zero and for late-time analysis it equals 1/3 (orthogonal system) or 1 (strata type), respectively.

Subscripts f and m refer to the fissures and matrix blocks, respectively.

Also, $n$ is the number of a normal set of fractures (1, 2 or 3) and $l$ is a characteristic dimension of a matrix block.

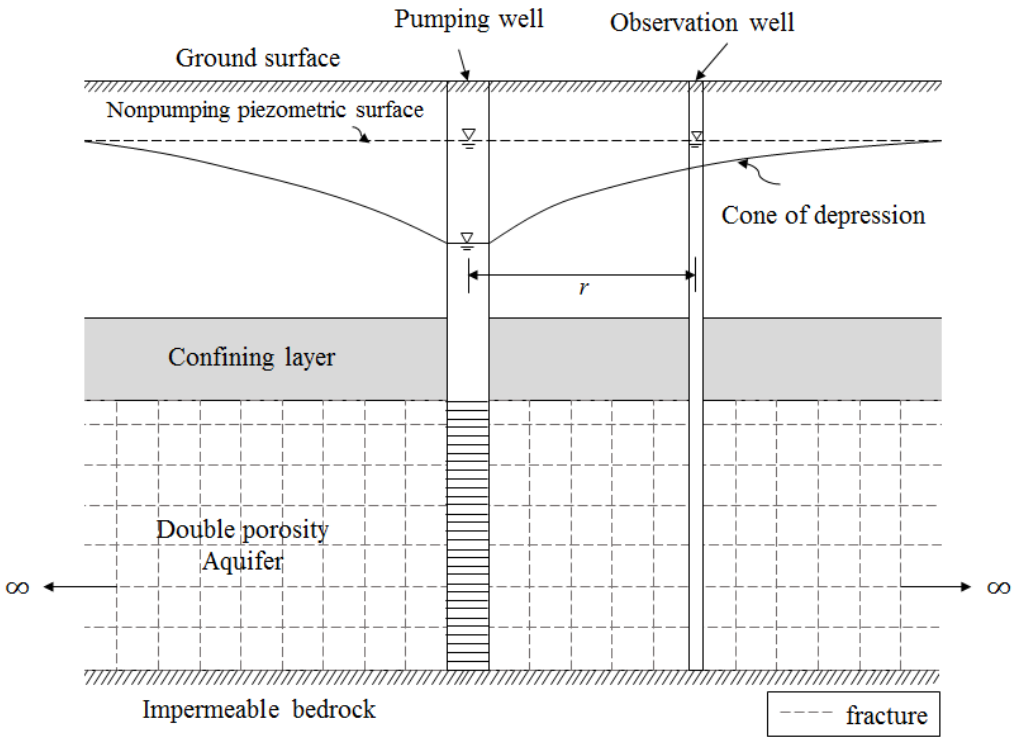


**Fig. 1** Schematic representation of a fractured double porosity aquifer with a fully penetrating pumping well

For small values of pumping time, Eq. (1) reduces to the Theis equation

$$s = \frac{Q}{4\pi T_{\mathrm{f}}} \mathrm{W}(u) \tag{8}$$

where,

$$u = \frac{(S_{\mathrm{f}} + \beta S_{\mathrm{m}}) r^2}{4\, T_{\mathrm{f}}\, t} \tag{9}$$

Equation (8) explains only the drawdown behavior in the fracture system ($\beta$ equals zero). For the late time-drawdown data, Eq. (1) also reduces to the Theis equation, which now describes the drawdown behavior in the combined fracture and matrix block system ($\beta$ equals 1/3 or 1). According to the pseudo-steady state inter-porosity flow concept, when the matrix blocks start contributing flow to the fracture flow, the drawdown at intermediate pumping times is only a function of $\lambda$ and is independent of early and late-time drawdown behaviors.

$$s = \frac{Q}{2\pi T_{\mathrm{f}}} K_0\left(\sqrt{\lambda}\right) \quad (10)$$

where, $K_0(X)$ is the modified Bessel function of the second kind and of zero order.

Bourdet and Gringarten (1980) plotted $\mathrm{F}(u^*, \lambda, \omega)$ versus values of $u^*$ for different values of $\lambda$ and $\omega$ and constructed a family of type curves each labeled with separate $\lambda$ and $\omega$ values as represented in Fig. 2. Numerous combinations of $\lambda$ and $\omega$ values generate different type curves.

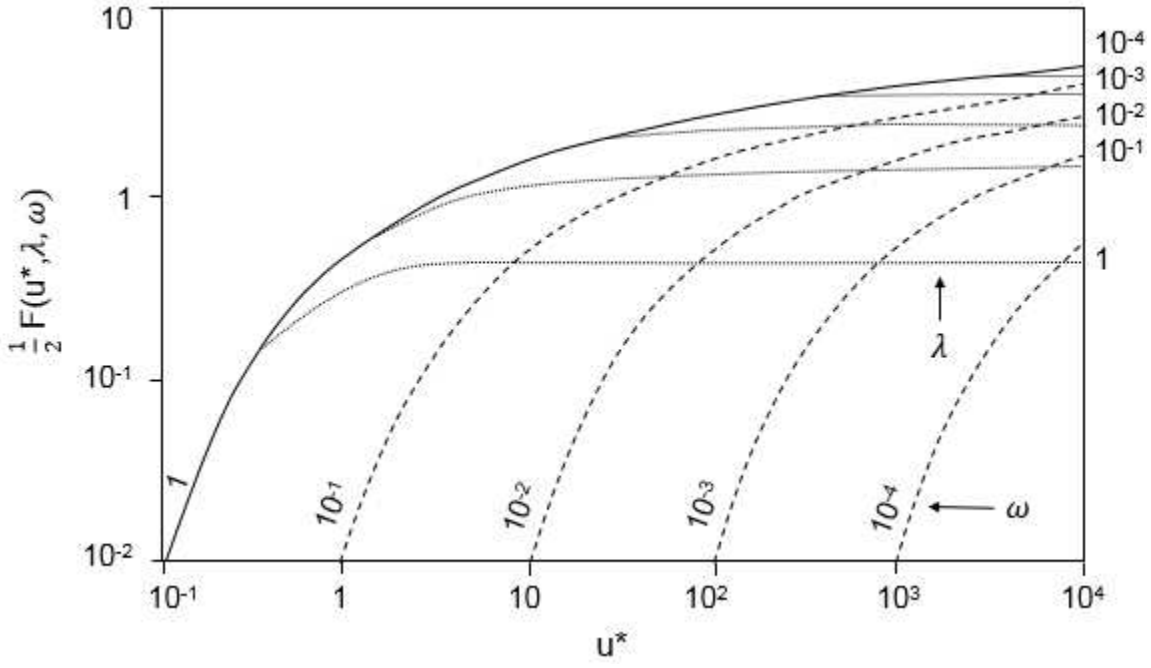


**Fig. 2** Family of Bourdet-Gringarten's type curves (1980), $\mathrm{F}(u^*, \lambda, \omega)$ versus values of $u^*$ for different values of $\lambda$ and $\omega$

To determine the double porosity confined aquifer parameter values ($T_{\mathrm{f}}$, $S_{\mathrm{f}}$, $S_{\mathrm{m}}$, $\lambda$, and $\omega$), time-drawdown data recorded in a pumping test is plotted on logarithmic paper of the same scale as for the type curves (Fig. 2). The time-drawdown field data curve is superimposed on the type curves, keeping the coordinate axes of the two plots parallel and adjusted until most of the plotted points of the observed early time-drawdown data match on one of the type curves with a $\lambda$.

A match point is selected and its coordinates on both plots are recorded $[(\frac{1}{u})_{\mathrm{m}}, \mathrm{W}(u)_{\mathrm{m}}, s_{\mathrm{m}}, t_m]$. With values of the match point coordinates thus determined, aquifer parameters ($T_{\mathrm{f}}$ and $S_{\mathrm{f}}$) are obtained from Eqs. (8) and (9), $(\beta = 0)$. If the plotted data exhibit a horizontal straight-line segment or only an inflection point, the value of the stabilized drawdown or that of the drawdown at the inflection point is substituted into Eq. (10) and $\lambda$ is calculated.

The late time-drawdown data are then superposed on the type curves, keeping the coordinate axes of the two plots parallel and adjusted until most of the plotted points of the observed late time-drawdown data match on one of the type curves with an $\omega$. From the second match point, $[(\frac{1}{u})_{\mathrm{m}}$, $\mathrm{W}(u)_{\mathrm{m}}, s_{\mathrm{m}}, t_{\mathrm{m}}]$ and by using Eq. (8) and (9), values of $T_{\mathrm{f}}$, $S_{\mathrm{f}}$, $S_{\mathrm{m}}$, and $\omega$ can be determined.

The process of curve matching is rather subjective and involves graphical error. In the next section an ANN model is developed as an alternative to curve matching for the determination of double porosity fractured aquifer parameters.

## 3 Materials and methods

In the following sections we demonstrate the methodology of the network development in a clear and systematic procedure. The methodology consists of six steps and in each step the rationale on the choice of procedures and their advantages are discussed and documented.

***Step I: Generation and Selection of Input Data Patterns***

To generate (to select) the training data patterns for the network design, first a logical range of Log $(u^*)_{\mathrm{m}}$ (from -1 to 4), $\lambda_{\mathrm{m}}$ (from $10^{-9}$ to 1) and of $\omega_{\mathrm{m}}$ (from $10^{-4}$ to 1) parameters are selected as the ANN output targets that represent the aquifer behavior according to the type curve presented by Bourdet-Gringarten (1980) and as inferred from Fig. (2). Using interval values of 0.01, 0.05 and 0.05 for Log $(u^*)_{\mathrm{m}}$, $\lambda_{\mathrm{m}}$ and $\omega_{\mathrm{m}}$, respectively; 200000 sets of training input pattern each

constitutes $N$-1 elements ($N$ is the number of drawdown-time records) were generated as illustrated in Fig. 3.

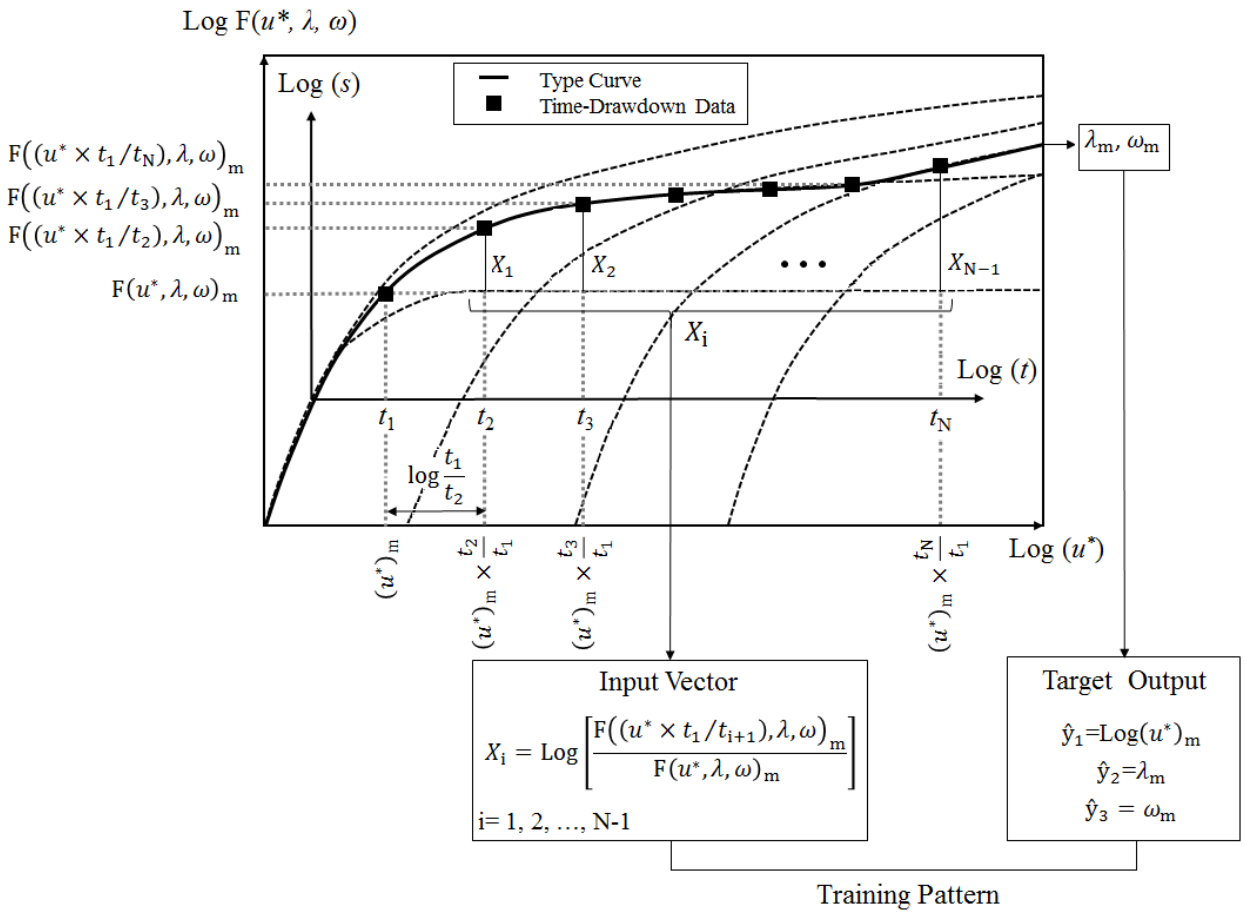


**Fig. 3** Graphical presentation of input vectors and target outputs generation for the training of the ANN

Therefore, the size of the input data matrix is [($N$-1) × 200000]. Then for all these sets of [Log $(u^*)_m$, $\lambda_m$, $\omega_m$], well function $F(u^*, \lambda, \omega)$ is calculated by Eq. (5) and then the training input patterns $X_i$ are generated by the following equation as illustrated in Fig. 3:

$$X_i = \log\left[\frac{F((u^* \times t_1/t_{i+1}), \lambda, \omega)_m}{F(u^*, \lambda, \omega)_m}\right] \quad (11)$$

Subscript m denotes the match point, i=1, 2, …, $N$-1 and $N$ is the number of time-drawdown records. Before using the generated training data patterns as input vector to the ANN, their

significance and the independence needs to be examined (Maier 2010). Data independency may be conducted by dimensionality reduction and filtering. Dimensionality reduction can be achieved by using PCA (Samani et al. 2007; Wu et al. 2014). Therefore, the training data patterns are normalized and subjected to PCA to reduce their dimensionality and eliminate redundant data.

PCA transforms the data to a new coordinate system such that the greatest variance by any projection of the data comes to lie on the first coordinate (called the first PC), and the second PC explains the maximum variances of the residual data set and so on. When the analysis is complete, the resulting components will display varying degrees of correlation with the observed variables, but are completely uncorrelated with one another. One of the parameters in PCA method is minimum fraction variance. By specifying a minimum fraction variance one can eliminate those principal components that contribute less than this value to the total variation in the data set and hence the dimensionality of the data set is reduced with no information lost (Cattell 1966).

Samani et al. (2007), Lin et al. (2010), Azari et al. (2015), Azari and Samani (2018) and later Tabari et al. (2021) applied PCA successfully to reduce the dimension of the input vector and develop a network with fixed structure for accurate determination of isotropic and anisotropic confined aquifer parameters, respectively.

***Step II: Selection of the Network Architecture***

A typical ANN consists of an input layer, a number of hidden layers and an output layer each having a number of processing neurons (nodes). The number of neurons in input and output layers is determined by the number of input and output variables, respectively. The number of hidden layers and their neurons are determined in the process of model training (calibration) usually by a trial-and-error procedure. The pattern of connection between nodes, the method of determining the connection weights, and the activation function characterizes the architectures of the network

(Fausett 1994; ASCE 2000a, 2000b). ANNs are also categorized based on the direction of information flow and processing (Maier et al. 2010). For instance, in a feed-forward neural network, also known as multi-layer perceptrons (MLP) information passes from the input nodes to the output nodes only (Hornik 1989; Tabari and Zarif Sanayei 2019). This is in contrast to a recurrent ANN in which information flows through the nodes in both directions, from the input to the output nodes and vice versa (Malekpour and Tabari 2020). Feed forward neural networks are the most commonly used ANN architecture (ASCE 2000a; Maier et al 2010; Wu et al. 2014). A single-hidden-layer feed forward neural network is sufficient to approximate any continuous mapping from the input patterns to the output mainly because they are less susceptible into poor local minima (Razavi and Tolson 2011). Fig. 4 illustrates the architecture of our single-hidden-layer network before and after conducting PCA on the input data sets. The optimum number of neurons in the hidden-layer is determined in the process of network training (calibration) in the next sections where the optimum structure of the network is also determined.

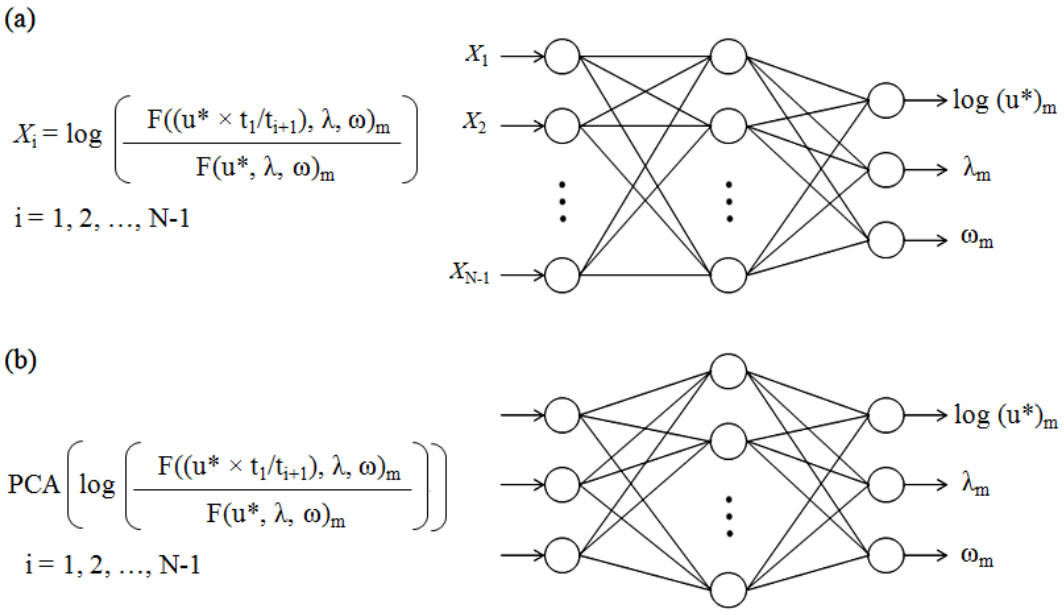


**Fig. 4** Structure of the single-hidden-layer network before (a) and after (b) conducting PCA on the input training data sets

***Step III: Network Training (Calibration)***

Among various methods for neural network training or calibration, the classic back-propagation (BP) method developed by Rumelhart et al. (1986) among others is the most popular for it can learn the mapping of any linear and nonlinear relationship between the inputs and outputs (Maier and Dandy 1999, 2000; ASCE 2000a) by finding the optimum set of weights with the use of an optimization algorithm.

In the BP method, the inputs are delivered to the hidden-layer after being multiplied by synaptic weights. The output of the hidden-layer ($h_l$) can be obtained based on the following equations:

$$Z_l = b_l + \sum_{i=1}^{n} X_i \, w_{il} \quad (12)$$

$$h_l = f(Z_l) \quad (13)$$

where, $X_i$ is the input to the processing nodes (determined in Eq. (11) and subjected to PCA); $b_l$ is the bias representing the threshold value associated with node $l$; $w_{il}$ is the connection weight from the $i^{th}$ node in the preceding layer to node $l$ for imitating the biological synapse strength; n is the total number of inputs applied to nodes i in the input layer and $f$ is the activation function for converting the weighted summation input to the output.

Different implementations of the conjugate gradient approach and various quasi-Newton implementations have been incorporated into the BP algorithm to enhance the convergence speed of this algorithm. While the global optimization algorithms such as genetic algorithm are less prone to fall in local optima they are more computationally expensive and often have more parameters that need to be determined (Haykin 1999; Wu et al. 2014).

In this paper, the network training and the weights adjustment are implemented by the deterministic Levenberg–Marquardt (LM) optimization method which is probably the most efficient optimization method for small and medium sized neural networks (Razavi and Tolson

2011). Many researchers have successfully used this methodology to hydrology problems (Samani 1990; Maier and Dandy 1999, 2000; Coulibaly et al. 2001; Daliakopoulos et al. 2005; Samani et al. 2007; Soltani and Tabari 2012; Azari et al. 2015; Azari and Samani 2018). In the LM algorithm, the updated function of the weights $w(k+1)$ is estimated using:

$$w(k+1) = w(k) - [J^{\mathrm{T}} \times J + \mu I]^{-1} \times J^{\mathrm{T}} \times e \quad (14)$$

where, $J$ is the Jacobin matrix of the performance (error) criteria to be minimized, $\mu$ is the learning rate, $k$ is the iteration during the optimization process, $e$ is the vector of the residual value and $I$ is the identity unit matrix. After, the weights and biases are adjusted for all the interconnection neurons in different layers and the convergence criterion is reached (e.g. $10^{-6}$), network training is complete.

***Step IV: Determination of Network Optimum Structure***

To make sure that the network structure designed in the calibration section is the optimum structure of the network (i.e., the optimization algorithms have not fallen in a local optimum point), a sensitivity analysis is conducted to determine the optimum number of hidden layers and nodes. This will put further confidence on generalization of the trained network (structural validity, Wu et al.2014) in predicting the match point coordinates (network target). In the sensitivity analysis error measures (the difference between the expected target and the simulated target) such as absolute errors, squared errors, relative errors, product differences and information criteria may be used (Maier et al. 2010). In this paper the following two efficiency criteria are used:

- The relative root mean square error (RRMSE) of the calculated target:

$$\mathrm{RRMSE} = 100 \times \sqrt{\frac{1}{\mathrm{n}} \sum_{\mathrm{j}=1}^{\mathrm{n}} \left(\frac{\hat{y}_{\mathrm{j}} - y_{\mathrm{j}}}{y_{\mathrm{j}}}\right)^2} \quad (15)$$

where, $\hat{y}_j$ is the simulated target calculated by the network, $y_j$ is the actual target, and n is the number of data patterns. The accuracy of prediction increases as the value of RRMSE decreases. RRSME=0 indicates 100% precision.

- The determination coefficient, $R^2$:

$$R^2 = 1 - \frac{\sum(y_j - \hat{y}_j)^2}{\sum y_j{}^2 - \frac{\sum \hat{y}_j}{n}} \quad (16)$$

where, $R^2$ is a key output of regression analysis that indicates how well the network output fit the actual output. $R^2$=1 indicates 100% fit between network output values and expected target values. The advantage of RRMSE and $R^2$ that are used in this work is that their values vary between 0 to 100% and 0 to 1, respectively and in general sense they are more understandable and are unambiguous measure of average error magnitude.

***Step V: Testing the Developed Network***

Having developed the network with the optimum topology the test patterns are used to assess its performance in determining the match point coordinates and hence the aquifer parameters. The best result of network performance is obtained when the trained network produces the smallest prediction error on the test data sets which are different from the training sets.

The performance of the trained network was assessed by 100000 sets of synthetic error-free drawdown data. The synthetic data are generated by Bourdet-Gringarten's analytical solution (Eq. (1) to (5)) for the double porosity aquifer from combinations of idealized $T_f$, $S_f$, $S_m$, $\lambda$ and $\omega$ values ranging from $10^2$ to $10^6$ $m^2$/day, $10^{-6}$ to $10^{-3}$, $10^{-3}$ to $10^{-1}$,$10^{-9}$ to 1.0 and $10^{-4}$ to 1.0, respectively by selecting a number of time steps as on Fig. 3. These synthetic error-free data (they are error-free because Eq. (1) to (5) are exact analytical solution of double porosity aquifers response to pumping) were converted to drawdown ratios using Eq. (17) which forms the input testing vectors ($X_i$) to the developed ANN.

$$X_i = \log(s_{i+1}) - \log(s_1) = \log\left(\frac{s_{i+1}}{s_1}\right) \quad (17)$$

where, $s_i$ is the drawdown recorded at time $t_i$.

Applying the PCA to the input vectors ($X_i$), the reduced drawdown ratios PCA $\left[\log\left(\frac{s_{i+1}}{s_1}\right)\right]$ are generated. Figure 5 illustrates the structure of the developed network at the testing stage. The developed network receives the reduced drawdown ratios (drawdown ratios subjected to PCA) and calculates the Log $(u^*)_m$, $\lambda_m$, and $\omega_m$ which are converted to $T_f$, $S_f$, and $S_m$ by Eq. (1) to (5).

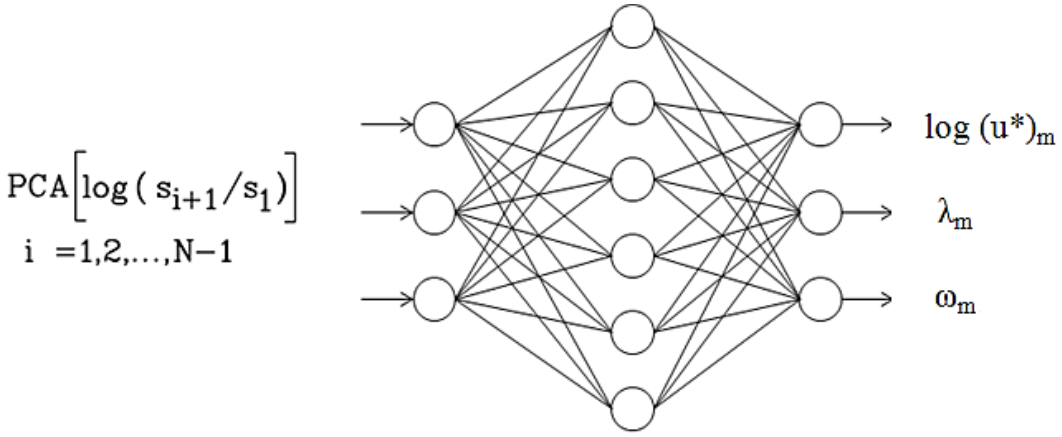


**Fig. 5** Structure of the developed ANN in the testing stage

***Step VI: Validation of the developed Network***

The main goal of model validation is establishing greater confidence in the model in producing/predicting system actual response. In other words, the model should be physically plausible as well as being predictive. Therefore, in this step, two sets of real pumping test (time-drawdown) data were used to evaluate the applicability and reliability of the developed ANN. The first set is adapted from Moench (1984) and the second set from McConnell (1993):

*a) First Pumping Test*

298 This pumping test was carried out in the fractured Tertiary volcanic rocks of the Nevada Test Site,
299 U.S.A., as published by Moench (1984) that is pumped by a fully penetrated well at a constant rate
300 of 35.8 l/s for nearly 3 days. Like Moench, we assume that the fractured aquifer is the strata type
301 (i.e., $\beta$ = I). The time-drawdown data for an observation well 110 m away from the pumping well
302 are listed in Table S1 (supplemental materials).
303 *b*) *Second Pumping Test*
304 This test is conducted in a double porosity aquifer of the strata type (i.e., $\beta$ = I) at Kingdom City,
305 Missouri which is a small community in the Ozark region. A 1500 minute well test runs on the
306 Kingdom City well in 1988 at a constant rate of 500 gpm. The time-drawdown data from this test
307 are given in Table S2 (supplemental materials).
308 Each drawdown data set is converted to drawdown data ratios and subjected to PCA. The reduced
309 data set is used as the input to the developed network and allowed the network to determine the
310 match point coordinates values $[(u^*)_{\mathrm{m}}, \lambda_{\mathrm{m}}$ and $\omega_{\mathrm{m}}]$.
311

312 **4 Results and discussion**

313 In order to determination of the fractured double porosity aquifer parameters ($T_{\mathrm{f}}$, $S_{\mathrm{f}}$, and $S_{\mathrm{m}}$), the
314 six-step protocol based on multi-layer perceptron (MLP) networks architecture were proposed and
315 implemented. Based on these steps, the following actions were performed:
316 generation of the required data for neural network training and testing within the defined allowable
317 range, reduction the dimensions of the input parameters with PCA, determination of the optimal
318 network structure, training of developed simulation model and evaluation of the network
319 performance for two sets of real pumping test.

320 Based on step I of developed methodology, Table 1 provides PCA parameters for the training
321 patterns Xi (generated by Eq. (11)). The principal components were extracted by considering
322 minimum fraction variance of 0.001%. The result of PCA given in Table 1 shows that the three
323 first principal components together describe 99.99993% of the variance of the training data sets.
324 Because the variance accounted by the fourth component is smaller than minimum fraction
325 variance (i.e., 0.000071<0.001) it is ignored.
326
327 **Table 1**. The principal component parameters of the training set for the double porosity aquifer

| Principal Component | Eigenvalue | Variance (%) | Cumulative variance (%) |
|---|---|---|---|
| PC1 | 61.669 | 94.87532 | 94.87532 |
| PC2 | 3.309 | 5.090766 | 99.96608 |
| PC3 | 0.022 | 0.033846 | 99.99993 |
| PC4 | 4.614e-05 | 7.10e-005 | 100 |
| PC5 | 1.186e-08 | 0 | 100 |

328
329 Moreover, the results of the screen test (Cattell 1966), as shown in Fig. 6, confirm that only the
330 three first principal components should be considered as input vectors. This is in harmony with the
331 well function that has three variables and also with the Bourdet-Gringarten's type curve which
332 consist of three segments. This means that the elements of training input vector reduce to 3 and
333 the number of neurons in the input-layer of the network to be designed can be fixed to 3 neurons
334 instead of number of records in drawdown-time data which varies from one pumping test to
335 another. In brief the application of PCA on Input data has the following advantages: it reduces

number of neurons in both the input and hidden-layers, it reduces network training and testing times and it fixes the input-layer neuron independent of drawdown data records.

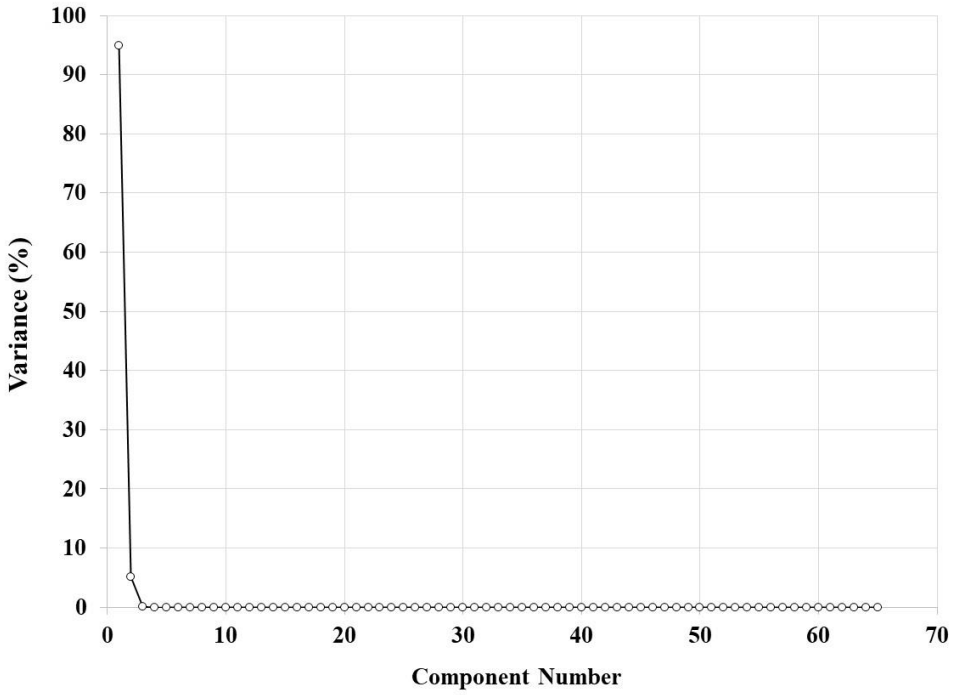


**Fig. 6** The scree plot of the training patterns

In step II, we started with a single-hidden-layer feed forward neural network. The number of nodes in input and output layers was already determined based on the three principal components of the training input data and the three variables in the Bourdet-Gringarten's well function of double porosity aquifers (i.e. the coordinates of match point, Log $(u^*)_m$, $\lambda_m$ and $\omega_m$). The inputs are fed through the input layer and, after being multiplied by synaptic weights, are delivered to the hidden layer. In the hidden and output layers an activation function such as threshold, unipolar sigmoid, bi-polar sigmoid, hyperbolic tangent, conic section, Gaussian and linear are used for converting the weighted summation input to the output (Haykin 1999). Based on our previous experience (Samani et al. 2007; Azari et al. 2015; Azari and Samani, 2018) we use, the hyperbolic tangent

function (tansig): $f(x) = (1 - e^{-2x})/(1 + e^{-2x})$ for the hidden layer and the linear transfer function (purelin): $[f(x) = x\,, \text{for all } x]$ for the output-layer (Fig. 1S, Supplementary materials). Tabari et al. (2011) also analyzed the performance of generalized MLP architectures using the above activation functions for the hidden and output layers. Simulation results showed that tansig (hyperbolic tangent) function performs better recognition accuracy than that of the other functions. According to the considered structure for ANN, single-hidden-layer network was calibrated (trained) using two automated parameter optimization schemes namely Particle Swarm Optimization (PSO) (Kennedy and Eberhart 1995) and Genetic algorithm (GA) (Davis 2002). Both algorithms resulted in a network with six nodes in the hidden layer. Therefore, the structure of the trained network gained the topology of [3×6×3], where in, 3, 6 and 3 refer to the number of neurons in the input, hidden and output layers, respectively (Fig. 7). The parameters applied during the training process are shown in Table 2.

In order to evaluate the optimal structure of the prepared neural network model, it is necessary to use the error index according to step four. Figure 8 shows variations of the error criteria (i.e., $R^2$ and RRMSE) with respect to number of hidden layers and number of nodes for the predicted values of the three network targets. The four plots in Fig. 8 collectively indicate that a single-hidden-layer feed forward network with the topology of [3×6×3] is the best and optimum ANN that efficiently model the well function of double porosity aquifers and accurately predict the match point coordinates. The values of the above two criteria for the developed optimum network are also indicated on Fig. 8.

Figure 9 is a plot of convergence of BP indicating that the network with the topology of [3×6×3] is trained smoothly and quickly without falling to local optima compare to networks with simpler and complicated topologies, i.e., [3×3×3], [3×9×3], [3×12×3] and [3×13×3].

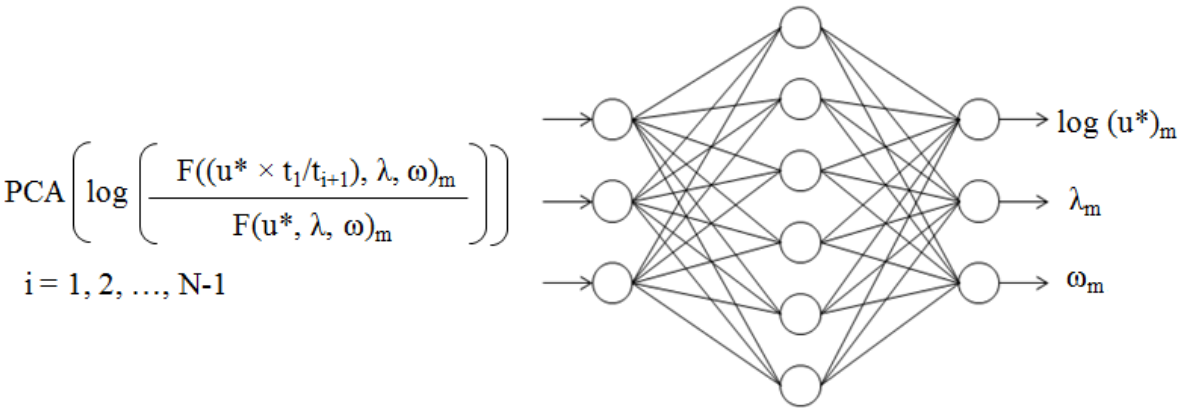


373

374 **Fig. 7** The optimum structure of the trained ANN

375

376 **Table 2**. The ANN parameters applied during training

| Parameter | Value |
|---|---|
| Learning rate | 0.5 |
| Convergence criterion | 1e-6 |
| Maximum training cycle | 10000 |
| Number of training patterns | 200000 |

377

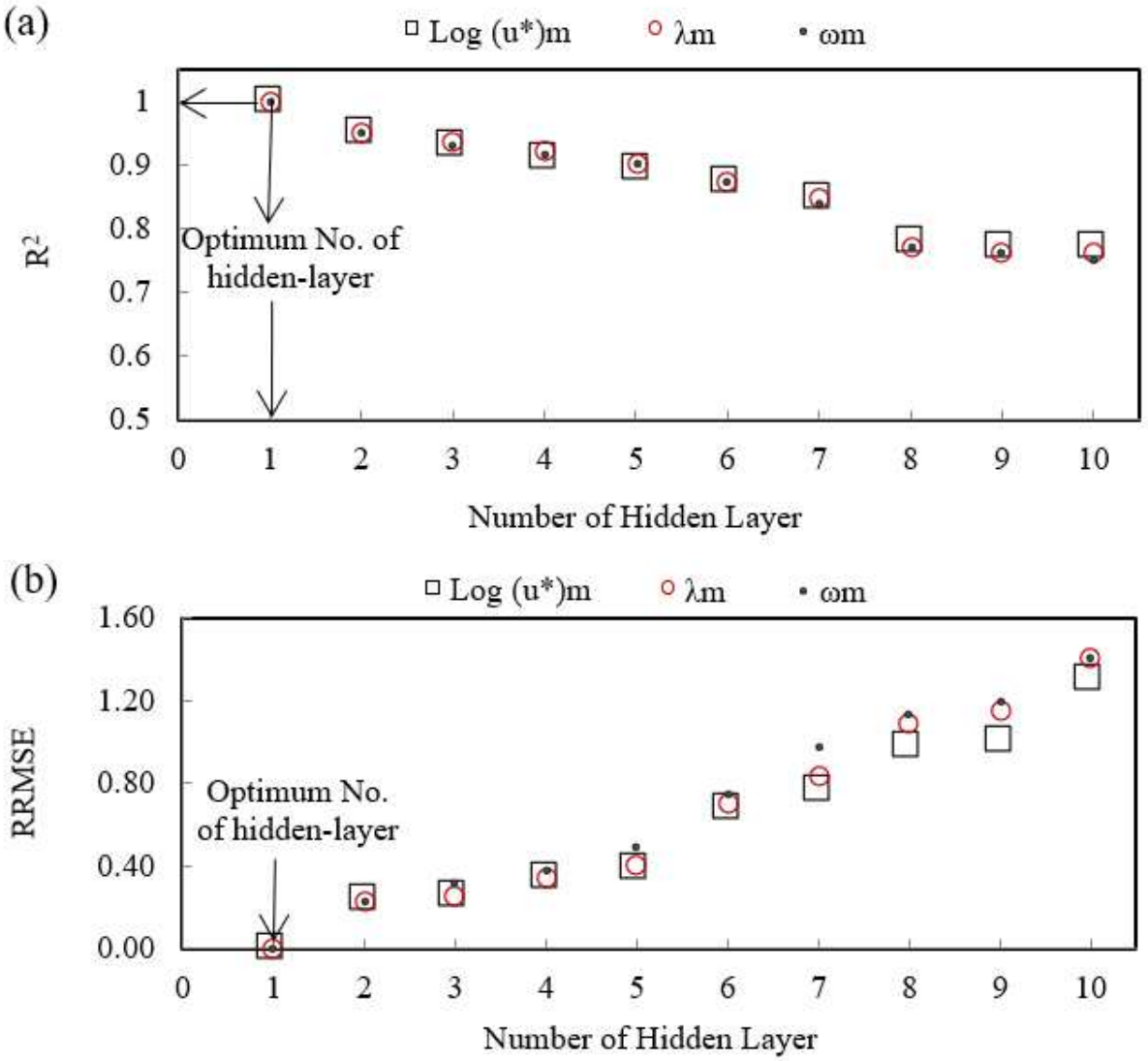


**Fig. 8** Sensitivity plots based on number of hidden layer and number of hidden neurons for the developed ANN model structure

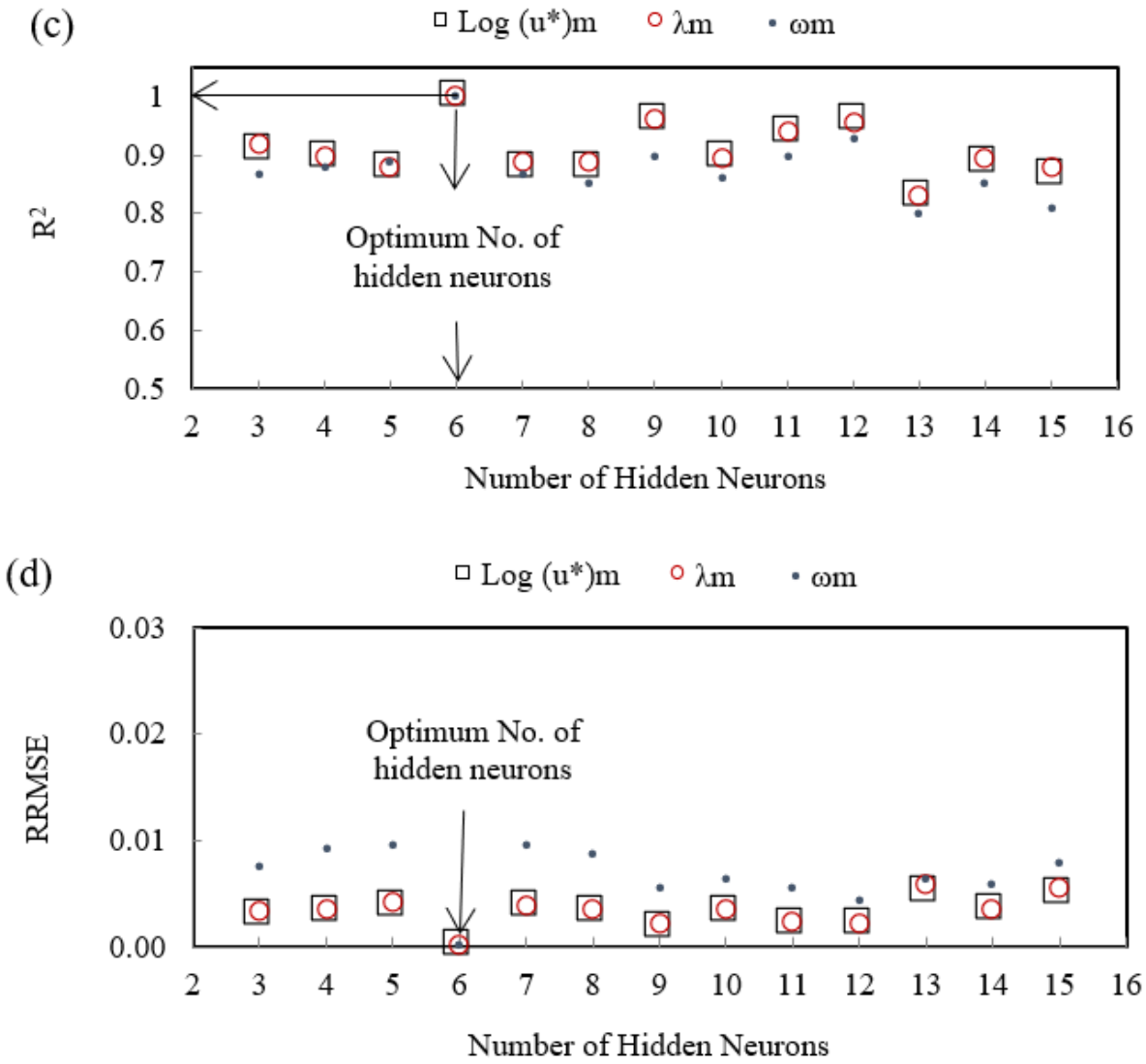


381

382 **Fig. 8** (continue)

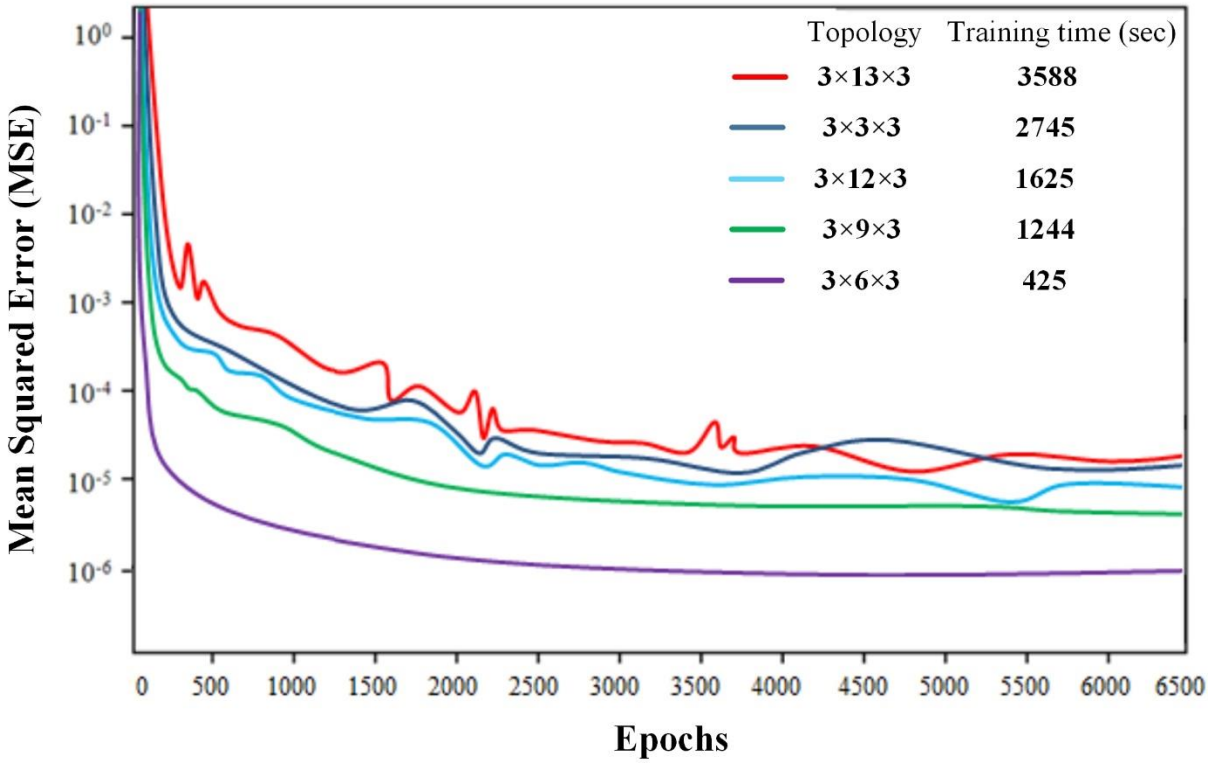


**Fig. 9** Convergence plot of networks with different topology

By applying the test stage data to the developed optimal neural network topology, the network performance was evaluated. Figure 10 shows the scatter plots and the best-fitted line as well as the QQ (normal distribution) plot of residuals (Bennett et al. 2013) for the idealized and estimated aquifer parameters ($T_f$, $S_f$, and $S_m$) by the proposed ANN for the double porosity aquifer, respectively. As shown in these figures, the developed network can accurately estimate the aquifer parameters over a wide tested range. In all plots the value of $R^2$ is equal to unity and RRMSE values are very close to zero (summarized in Table 3) indicating a high prediction precision of the developed network in simulating the exact theoretical response of the real system (Eq. (1)) and hence its replicative validity (Wu et al. 2014).

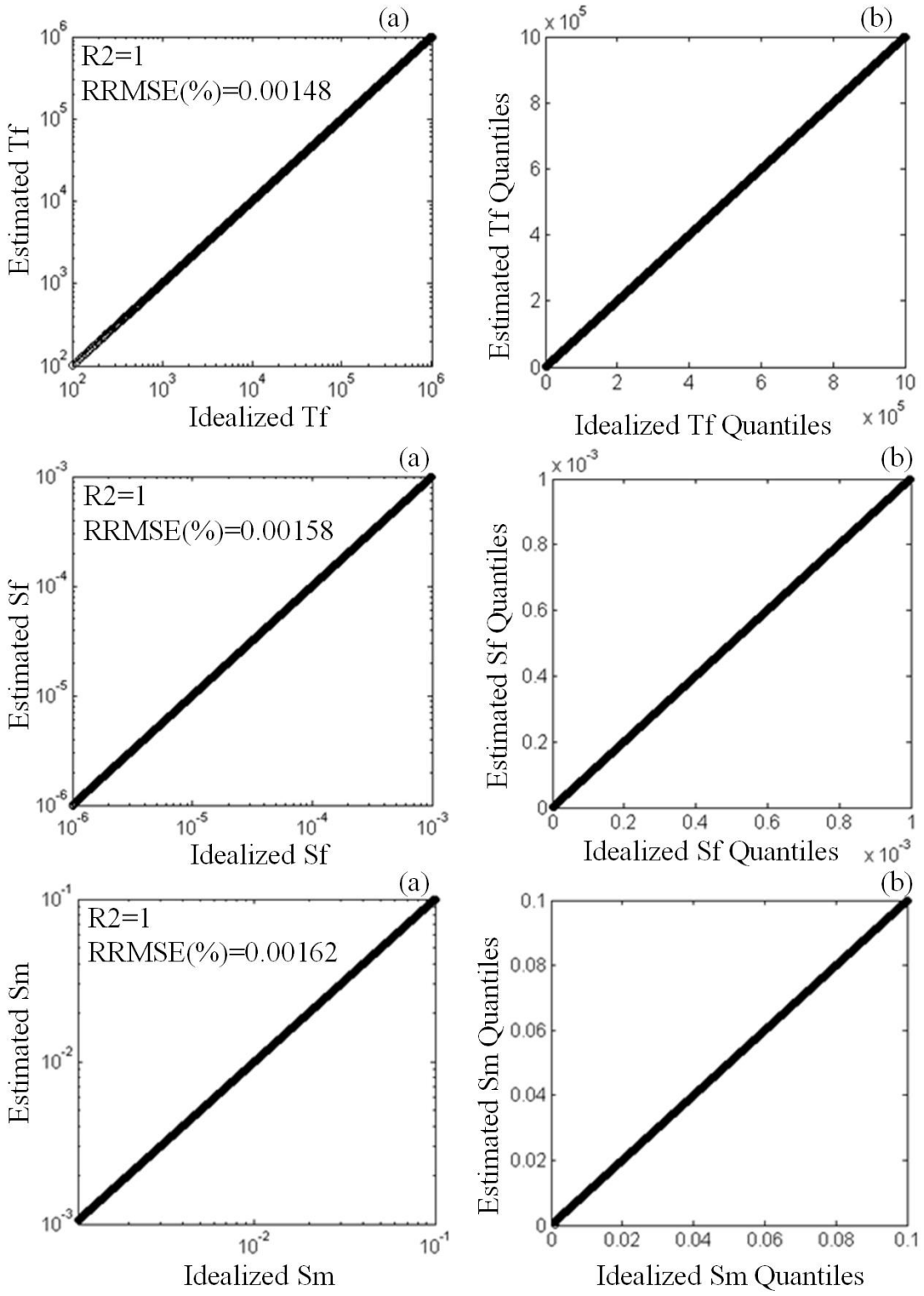


396

397 **Fig. 10** a) Idealized versus calculated aquifer parameter values ($T_f$, $S_f$, and $S_m$), b) QQ plot of

398 residuals

399 **Table 3.** Values of the RRMSE (%) and $R^2$ of $T_f$, $S_f$, $S_m$, $\lambda$, and $\omega$ for the developed ANN during

400 the testing process

| Parameters | RRMSE (%) |
|---|---|
| $T_f$ | 0.00148 |
| $S_f$ | 0.00158 |
| $S_m$ | 0.00162 |
| λ | 0.00191 |
| ω | 0.00188 |

$R^2$=1 for the five above parameters

401

402 By implementing the proposed neural network model on two sets of time-drawdown real pumping
403 test, the model was validated. Table 4 compares the values of match point coordinates generated
404 by the developed network with those of type curve matching techniques given by Moench (1984)
405 and McConnell (1993) and for the first and second set of time-drawdown data, respectively.

406

407 **Table 4.** Values of the match points coordinates determined by the developed ANN and the type-

408 curve matching method for the double porosity aquifer

| Pumping test | Match point coordinates | Methods | |
|---|---|---|---|
| | | Type-curve Method | Developed ANN |
| First (Moench, 1984) | Log $(u^*)_m$ | 0.43 | **0.1** |
| | $\lambda_m$ | $7.3\times10^{-6}$ | **$4\times10^{-6}$** |
| | $\omega_m$ | 0.011 | **0.02** |
| Second (McConnell, 1993) | Log $(u^*)_m$ | 3.37 | **1** |
| | $\lambda_m$ | $1\times10^{-6}$ | **$2.5\times10^{-6}$** |
| | $\omega_m$ | 0.07 | **0.31** |

### 4.1 Determination of Aquifer Parameter Values

Having determined the match point coordinates of both pumping test data by the developed network, they are adjusted and extended for all time-drawn records as illustrated in Fig. 3:

$$\hat{y}_1 = \log(u^*)_j = \log\left[(u^*)_m \times \left(\frac{t_j}{t_1}\right)\right] , \; j = 1, 2, \dots, N \tag{18}$$

$$(u^*)_j = \left[(u^*)_m \times \left(\frac{t_j}{t_1}\right)\right] = 10^{\hat{y}_1} \tag{19}$$

$$F[(u^*)_j, \lambda_m , \omega_m] = F\left(10^{\hat{y}_1}, \hat{y}_2, \hat{y}_3\right) \tag{20}$$

$$s_m = s_j \tag{21}$$

$$t_m = t_j \tag{22}$$

Substituting these values of the match point coordinates into Eq. (1) to (5) the double porosity aquifer parameter values ( $T_f$ , $S_f$ , and $S_m$ ) are determined. The drawdown record point $\left[(u^*)_j , F_j, s_j, t_j\right]$ that yields the minimum RRMSE of the estimated drawdown compare to the real drawdown records is selected as the optimal match point coordinates which yields the aquifer parameter values with the greatest possible accuracy.

Aquifer parameter values ($T_f$, $S_f$, and $S_m$) determined by the developed network is given in Tables (5) and (6) for the first and second pumping tests, respectively, and compared with the corresponding values determined with the type curve matching technique. The RRSME values (5.72% and 9.78% compare to 0.02% and 0.03% for the first and second pumping tests) show higher precision for the proposed model. In the first and second pumping test, the fourteenth and eighth time-drawdown records were found to be the optimal points as they produce the lowest value of RRMSE (Fig. 11). The results in Tables (5) and (6) demonstrate the predictive validity of the developed network as it has been able to simulate the response of the real system very accurately.

**Table 5.** Aquifer parameter values estimated by the developed ANN and the type-curve matching method and their RRMSE (First pumping test)

| Aquifer parameters | Methods | |
|---|---|---|
| | Type-curve graphical Method (Moench, 1984) | Developed ANN |
| $T_f$ ($m^2$/day) | 333 | 393.82 |
| $S_f$ | 0.0016 | 0.0033 |
| $S_m$ | 0.15 | 0.1594 |
| RRMSE (%) | 5.72 | 0.02 |

**Table 6.** Aquifer parameter values estimated by the developed ANN and the type-curve matching method and their RRMSE (Second pumping test)

| Aquifer parameters | Methods | |
|---|---|---|
| | Type-curve graphicalMethod (McConnell, 1993) | Developed ANN |
| $T_f$ (gpd/ft) | 3661 | 3850 |
| $S_f$ | $10^{-5}$ | $4.5\times10^{-5}$ |
| $S_m$ | $1.2\times10^{-4}$ | $10^{-4}$ |
| RRMSE (%) | 9.78 | 0.03 |

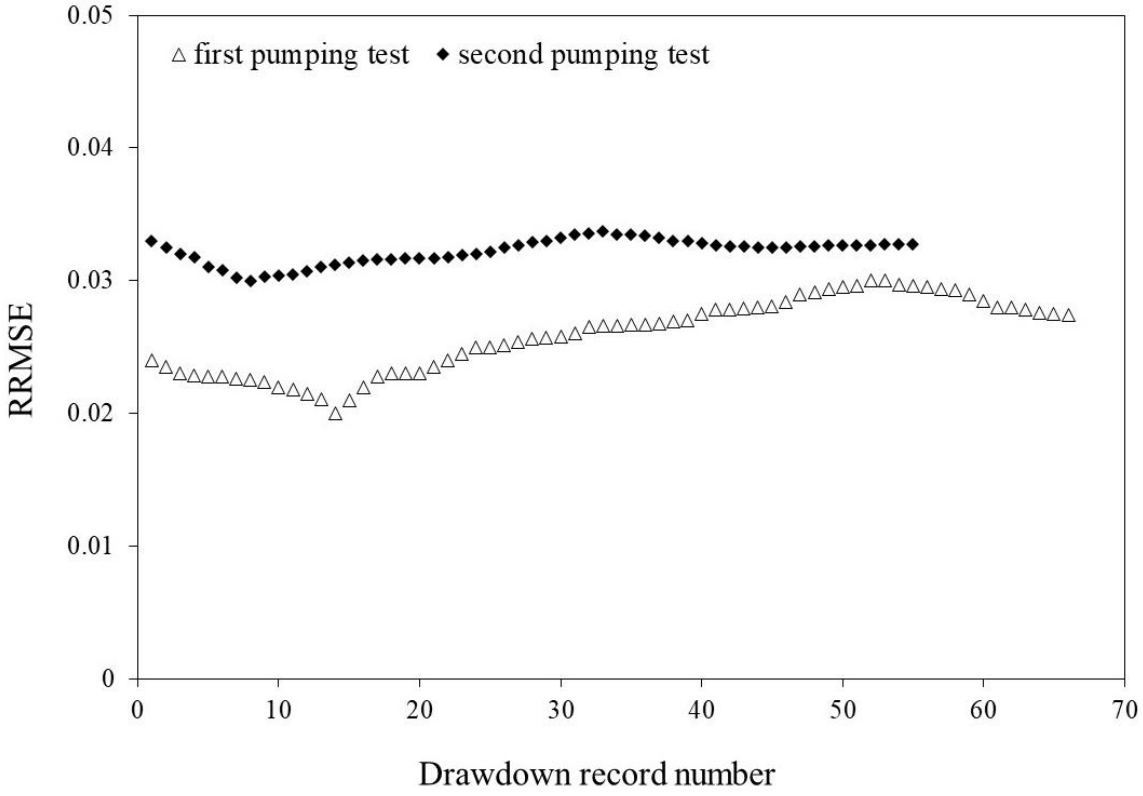


437

438 **Fig. 11** RRMSE plot locating the optimum drawdown-time record for the two sets of real

439 pumping test data.

440

441 **5 Summary and Conclusions**

442 In this paper, a single-hidden-layer feed forward neural network with the Levenberg-Marquardt

443 (LM) training algorithm was developed to imitate Bourdet-Gringarten's well function for the

444 determination of the double porosity aquifer parameters. We followed a six-step protocol similar

445 to that suggested by Wu et al. (2014) to develop the network and rationalized and documented the

446 methodology used in each step. In the first step (input data selection), *N*-1 sets of input data patterns

447 were generated using the exact analytical Bourdet-Gringarten's solution of flow in double porosity

448 aquifers by considering a wide range of logical values for the network output targets namely

449 $(u^*)_{\mathrm{m}}$, $\lambda_{\mathrm{m}}$and $\omega_{\mathrm{m}}$ (Fig. 3 and Eq. (11)). These three variables form neurons in the output-layer.

Before designing the network structure, the PCA was also applied on the training data sets to reduce the dimension of input training data patterns and eliminate the redundant data by considering a minimum fraction variance of 0.001%. It was found that the three first principal components together explain 99.99993% of the variance of the training data. As a result, the dimension of the input patterns and hence the number of neurons in the input-layer reduced and fixed to 3.

In the second step (selection of network architecture), we started with a single-hidden-layer network that is probably the most commonly used neural network in engineering applications. In this step activation functions were selected and an arbitrary number of neurons set for the hidden-layer.

In the third step (network calibration), the network training and weights adjustment were implemented by employing the classical BP training method and using the deterministic LM optimization algorithm. The network was trained with 6 neurons in the hidden-layer and gained the topology of [3×6×3] by maintaining the desired convergence criterion of $10^{-6}$ through a trial-and-error process.

In the fourth step (determining the network optimum structure), a sensitivity analysis was conducted to determine the optimum topology of the trained network by evaluating the ability of networks to generate the target output using the two efficiency criteria of RRMSE and $R^2$. It was found that both increasing and decreasing number of nodes in the hidden-layer and also increasing number of hidden-layer reduce the accuracy of the network to estimate the expected target. As a consequence, the optimum topology of the developed network was fixed to [3×6×3], regardless of the number of drawdown measurements.

In the fifth step (testing the network), the accuracy of the developed network was tested by 100000 synthetic error-free drawdown-time data sets. The scatter diagram of output targets (estimated target values versus actual target values) and the QQ plot of residuals indicated the network replicative validity. In the last step (network validation), the performance of the network in generating the match point coordinates is compared with the type curve matching technique using two sets of real pumping test data. The comparison evaluated by efficiency indices i.e. RRMSE and $R^2$ showed the predictive validity of the network structure.

In brief, the developed network receives the reduced drawdown ratios as inputs and provides the match point coordinates of the first record as the outputs. The outputs are incorporated with Bourdet-Gringarten's analytical solution for each individual time-drawdown records and aquifer parameters are calculated. Using each set of aquifer parameters, drawdown records are generated and compared with the real drawdown records, in terms of the RRMSE. The parameter values that give the lowest RRSME value are selected as the most accurate estimate of aquifer parameter values.

The results showed that the ANN model provides an automatic and fast procedure for aquifer parameters estimation and eliminates graphical error inherent in the type curve matching technique, therefore, the applicability of the ANN methodology is recommended as an efficient, accurate and easily used alternative tool to the graphical type-curve matching methods for the determination of double porosity aquifer parameters. The modeling procedure used in this paper may be used to design ANN models for other well functions in groundwater hydrology.

**Ethical Approval**

This article does not contain any studies with human participants or animals performed by any of the authors.

## Consent to Participate

Not Applicable

## Consent to Publish

Not Applicable

## Authors Contributions

Tahereh Azari: Conceptualization, Methodology, Data acquisition, Writing- Original draft preparation

Mahmoud Mohammad Rezapour Tabari: Conceptualization, Supervision, Methodology, Visualization, Editing of manuscript

## Funding

Not Applicable

## Competing Interests

The authors declare that they have no conflicts of interest.

## Availability of data and materials

Data and material would be made available on request.

## References

ASCE Task Committee on Application of Artificial Neural Networks in Hydrology (2000a) Artificial neural networks in hydrology, I: Preliminary concepts. Journal of Hydrology Engineering 5(2):115–123. https://doi.org/10.1061/(ASCE)1084-0699(2000)5:2(115)

ASCE Task Committee on Application of Artificial Neural Networks in Hydrology (2000b) Artificial neural networks in hydrology, II: Hydrologic applications. Journal of Hydrology Engineering 5(2):124–137. https://doi.org/10.1061/(ASCE)1084-0699(2000)5:2(124)

518 Azari T, Samani N, Mansoori E (2015) An artificial neural network model for the determination
519 of leaky confined aquifer parameters: an accurate alternative to type curve matching methods.
520 Iran Journal of Science and Technology 39(4):463-472.
521 https://doi.org/10.22099/IJSTS.2015.3389
522 Azari T, Samani N (2018) Modeling the Neuman's well function by an artificial neural network
523 for the determination of unconfined aquifer parameters. Computational Geosciences 22:1135–
524 1148. https://doi.org/10.1007/s10596-018-9742-8
525 Barenblatt GE, Zheltov IP, Kochina IN (1960) Basic concepts in the theory of seepage of
526 homogeneous liquids in fissured rocks. J Applied Mathematics Mechanics 24(5):1286-1303
527 Bennett ND, Croke BFW, Guariso G, Guillaume JHA, Hamilton SH, Jakeman AJ, Marsili-Libelli
528 S, Newham LTH, Norton JP, Perrin C, Pierce, SA, Robson B, Seppelt R, Voinov AA, Fath
529 BD, Andreassian V (2013) Characterising performance of environmental models. Environ
530 Model Software 40:1-20. https://dx.doi.org/10.1016/j.envsoft.2012.09.011
531 Boulton NS, Streltsova TD (1977) Unsteady flow to a pumped well in a fissured water bearing
532 formation. J Hydrology (35):257-270
533 Bourdet D, Gringarten AC (1980) Determination of fissure volume and block size in fractured
534 reservoirs by type-curve analysis. Paper SPE 9293 presented at the 1980 SPE Annual Fall
535 Techn Conf And Exhib., Dallas 1980
536 Cahyadi TA, Syihab Z, Widodo LE, Notosiswoyo S, Widijanto E (2021) Analysis of hydraulic
537 conductivity of fractured groundwater flow media using artificial neural network back
538 propagation. Neural Computing and Applications 33: 159–179.
539 https://doi.org/10.1007/s00521-020-04970-z

Cattell RB (1966) The scree test for the number of factors. Multivariate Behavioral Research 1(2):245-276. https://doi.org/10.1207/s15327906mbr0102_10

Coulibaly P, Anctil F, Aravena R, Bobee B (2001) Artificial neural network modeling of water table depth fluctuations. Water Resources Research 37(4):885–896. https://doi.org/10.1029/2000WR900368

Daliakopoulos IN, Coulibaly P, Tsanis IK (2005) Groundwater level forecasting using artificial neural networks. Journal of Hydrology 309(1–4):229–240. https://doi.org/10.1016/j.jhydrol.2004.12.001

Davis JC (2002) Statistics and Data Analysis in Geology, 3rd edn. Wiley, New York

Fausett L (1994) Fundamentals of neural networks. Prentice-Hall, Englewood Cliffs, NJ

Hantush MS, Jacob CE (1955) Non-steady radial flow in an infinite leaky aquifer. Trans American Geophys Union 36(1):95–100

Haykin S (1999) Neural Networks: A Comprehensive Foundation. Prentice-Hall, Englewood Cliffs

Hornik K, Stinchcombe M, White H. (1989) Multilayer feed forward networks are universal approximators. Neural Networks 2(5):359–366. https://doi.org/10.1016/0893-6080(89)90020-8

Kazemi H, Seth MS, Thomas GW (1969) The interpretation of interference tests in naturally fractured reservoirs with uniform fracture distribution. Society Petroleum Engineers Journal (246):463-472

Kennedy J, Eberhart R (1995) Particle swarm optimization, in: Proceedings of IEEE- International Conference on Neural Networks.; 4: 1942–1948. https://doi.org/10.1109/ICNN.1995.488968

562 Lin GF, Chen GR (2006) An improved neural network approach to the determination of aquifer
563 parameters. Journal of Hydrology 316(1–4):281–289.
564 https://doi.org/10.1016/j.jhydrol.2005.04.023
565 Lin GF, Chen GR (2005) Determination of aquifer parameters using radial basis function network
566 approach. Journal of the ChineseInstitute of Engineers 28(2):241–249.
567 https://doi.org/10.1080/02533839.2005.9670991
568 Lin HT, Ke KY, Chen CH, Wu SC, Tan YC (2010) Estimating anisotropic aquifer parameters by
569 artificial neural networks. Hydrological Processes 24(22):3237–3250.
570 https://doi.org/10.1002/hyp.7750
571 Maier HR, Dandy GC (1999) Empirical comparison of various methods for training feed-forward
572 neural networks for salinity forecasting. Water Resources Research 32(8):2591–2596.
573 https://doi.org/10.1029/1999WR900150
574 Maier HR, Dandy GC (2000) Neural networks for the prediction and forecasting of water resources
575 variables: a review of modeling issues and applications. Environmental Modelling and
576 Software 15(1):101–124. https://doi.org/10.1016/S1364-8152(99)00007-9
577 Maier HR, Jain A, Dandy GC, Sudheer KP (2010) Methods used for the development of neural
578 networks for the prediction of water resource variables in river systems: current status and
579 future directions. Environmental Modelling and Software 25(8):891–909.
580 https://doi.org/10.1016/j.envsoft.2010.02.003
581 Malekpour MM Tabari MMR (2020) Implementation of supervised intelligence committee
582 machine method for monthly water level prediction. Arabian Journal of Geosciences 13:1049.
583 https://doi.org/10.1007/s12517-020-06034-x

McConnell CL (1993) Double porosity well testing in the fractured carbonate rocks of the Ozarks. Ground water 31(1):75-83

Moench AF (1984) Double-porosity models for a fissured groundwater reservoir with fracture skin. Water Resources Research (20):831-846

Razavi S, Tolson BA (2011) A new formulation for feed forward neural networks. IEEE Transactions on Neural Networks 22(10):1588–1598. https://doi.org/10.1109/TNN.2011.2163169

Rumelhart DE, Hinton GR, Williams RJ (1986) Learning internal representations by error propagation. In: Rumelhart DE, David E, (Eds.), Parallel Distributed Processing MIT Press Massachusetts 318–362

Samani N, Gohari-Moghadam M, Safavi AA (2007) A simple neural network model for the determination of aquifer parameters. Journal of Hydrology 340(1–2):1–11. https://doi.org/10.1016/j.jhydrol.2007.03.017

Soltani J, Tabari MMR (2012) Determination of Effective Parameters in Pipe Failure Rate in Water Distribution System Using the Combination of Artificial Neural Networks and Genetic Algorithm. Journal of Water and Wastewater 23(83):2-15 (In Persian)

Samani N (1990) On the development and calibration of a parametric catchment sediment model. J Eng IRI 2(3):47-54

Sen Z (1988) Fractured Media type curves by double-porosity model of naturally fractured rock aquifers. Bull Techn Univ Istanbul (41):103-110

Tabari MMR, Ebadi T, Maknoon R (2011) Development of a Smart Model for Groundwater Level Prediction Based on Aquifer Dynamic Conditions Journal of Water & Wastewater 21(6):76-80 (In Persian)

607 Tabari MMR, Zarif Sanayei HR (2019) Prediction of the intermediate block displacement of the
608 dam crest using artificial neural network and support vector regression models. Soft
609 Computing 23(19):9629-9645
610 Tabari MMR, Azari T, Dehghan VA (2021) supervised committee neural network for the
611 determination of aquifer parameters: A case study of Katasbes aquifer in Shiraz plain, Iran.
612 Soft Computing 6(25):4785-4798. https://doi.org/10.1007/s00500-020-05487-2
613 Theis CV (1935) The relationship between the lowering of the piezometric surface and the rate
614 and duration of discharge of a well using ground-water storage. Trans Amer Geophys Union
615 16:519–524
616 Warren JE, Root PJ (1963) The behavior of naturally fractured reservoirs. Society Petroleum
617 Engineers Journal (3):245-255
618 Wu W, Dandy GC, Maier HR (2014) Protocol for developing ANN models and its application to
619 the assessment of the quality of the ANN model development process in drinking water quality
620 modeling. Environmental Modelling and Software 54:108–127.
621 https://doi.org/10.1016/j.envsoft.2013.12.016

# Figures

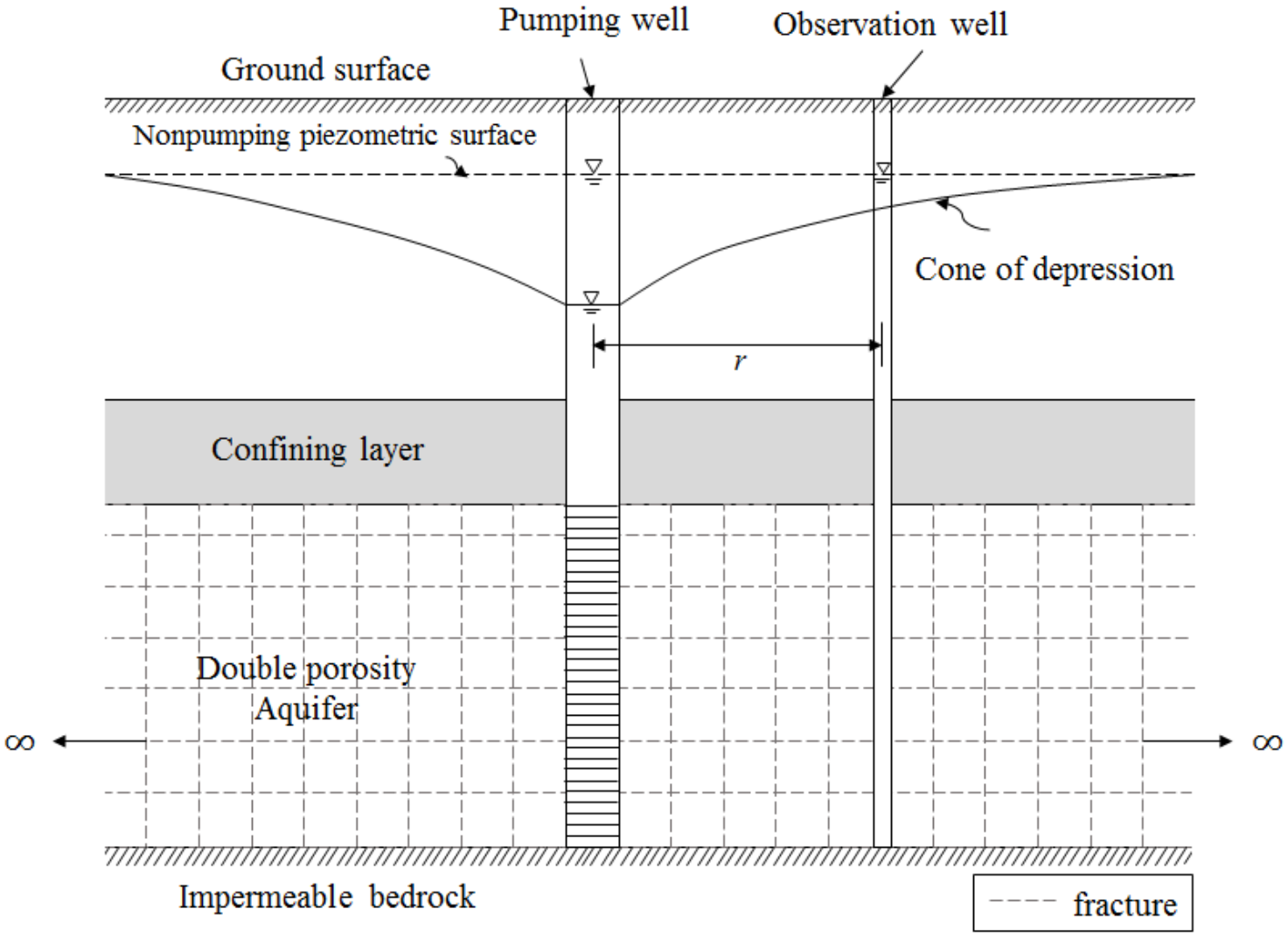


**Figure 1**

Schematic representation of a fractured double porosity aquifer with a fully penetrating pumping well

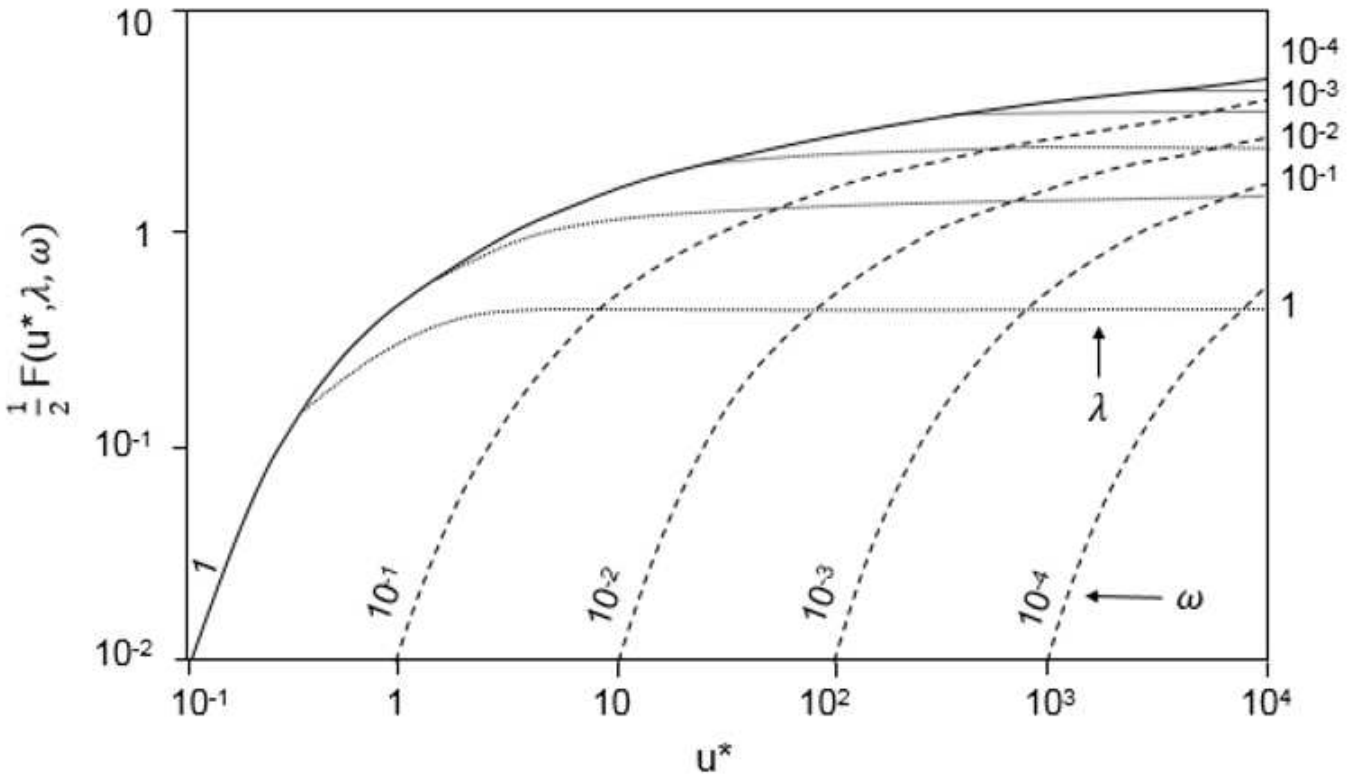


**Figure 2**

Family of Bourdet-Gringarten's type curves (1980), F(u^*,λ,ω) versus values of u^* for different values of λ and ω

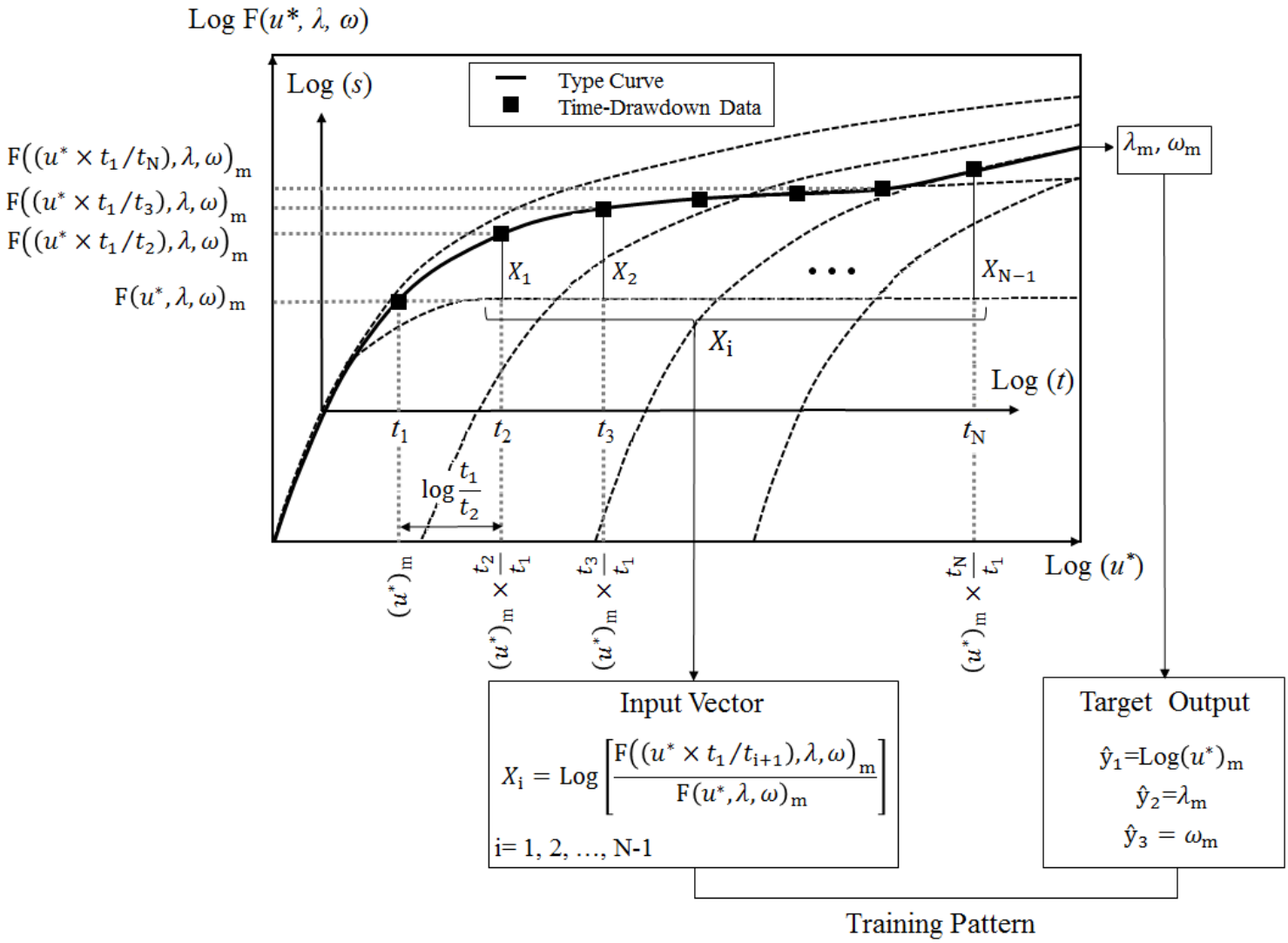


**Figure 3**

Graphical presentation of input vectors and target outputs generation for the training of the ANN

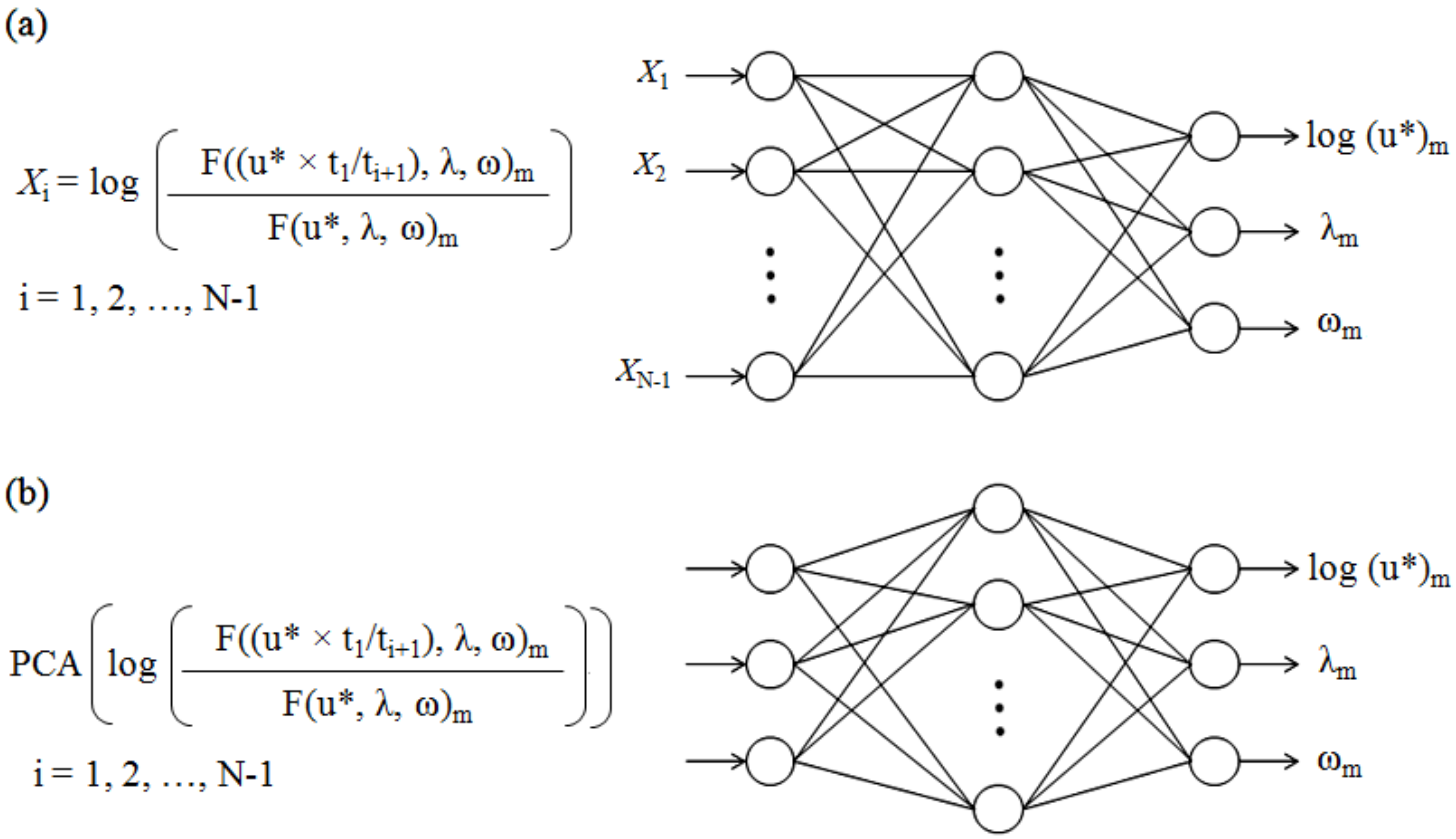


**Figure 4**

Structure of the single-hidden-layer network before (a) and after (b) conducting PCA on the input training data sets

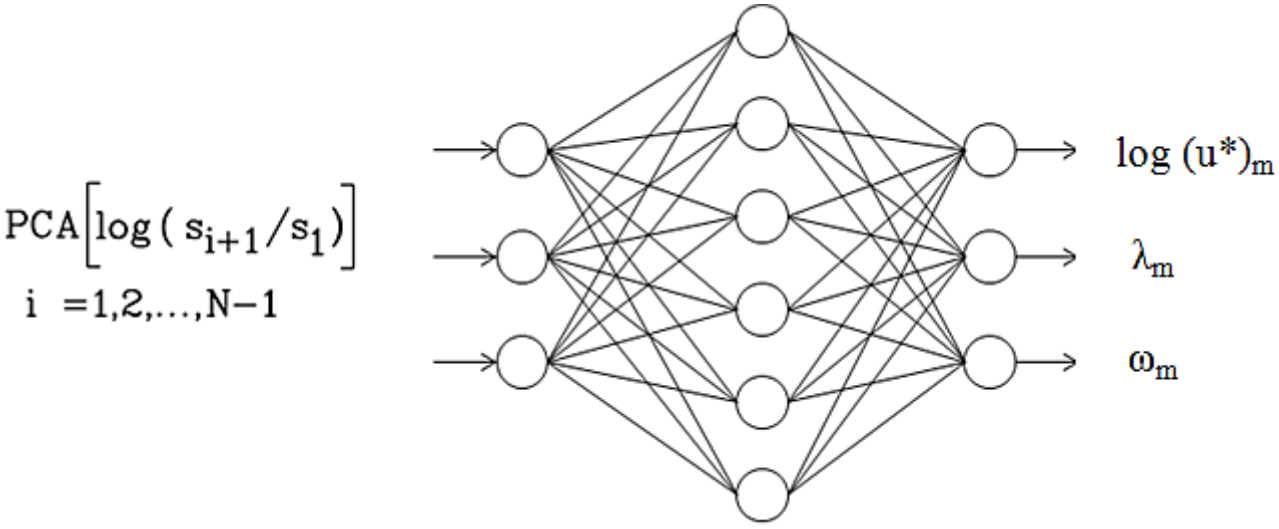


**Figure 5**

Structure of the developed ANN in the testing stage

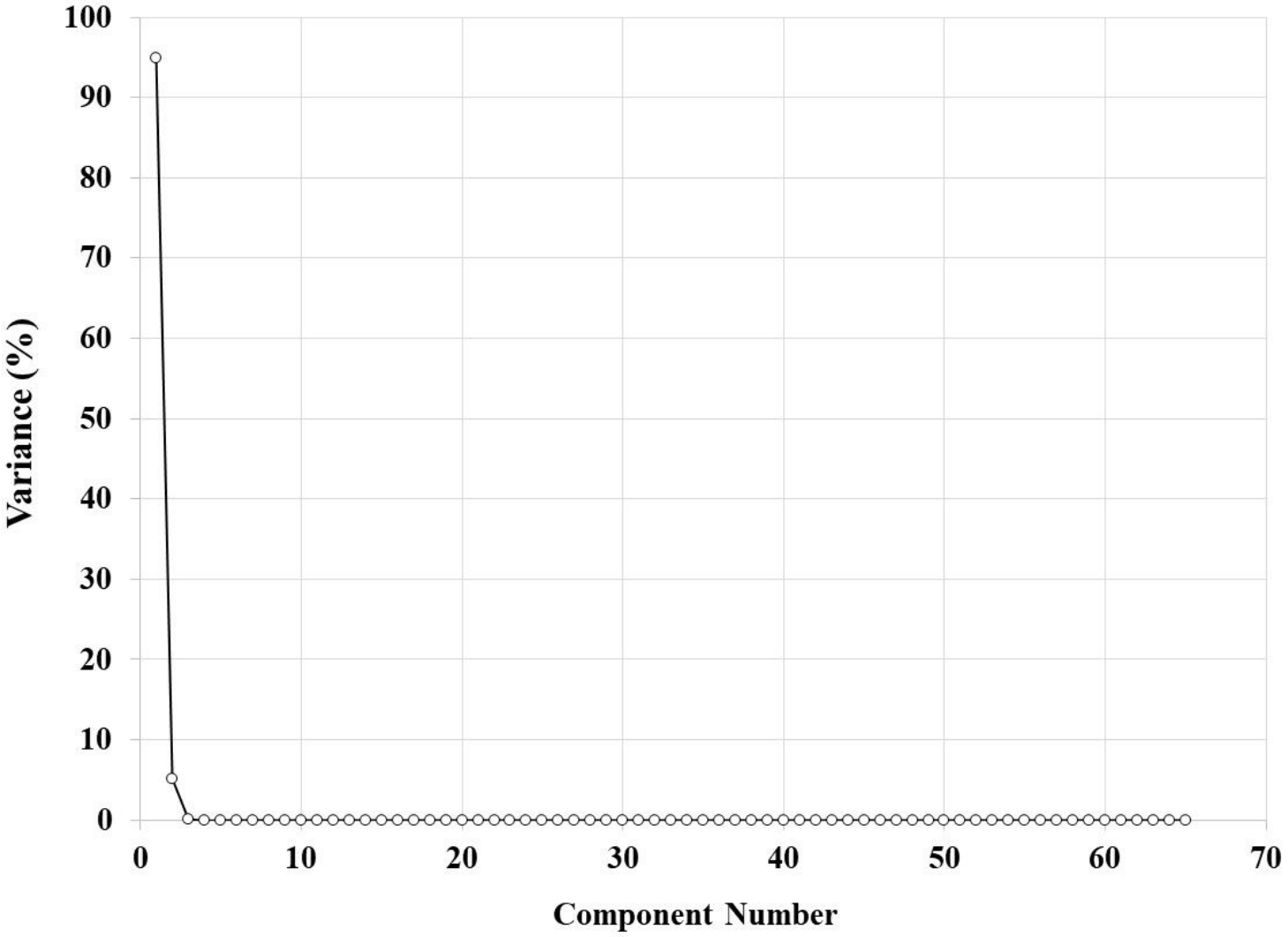


Figure 6

The scree plot of the training patterns

$$\mathrm{PCA}\left[\log\left[\frac{F((u^* \times t_1/t_{i+1}), \lambda, \omega)_m}{F(u^*, \lambda, \omega)_m}\right]\right]$$

$$i = 1, 2, \ldots, N\text{-}1$$

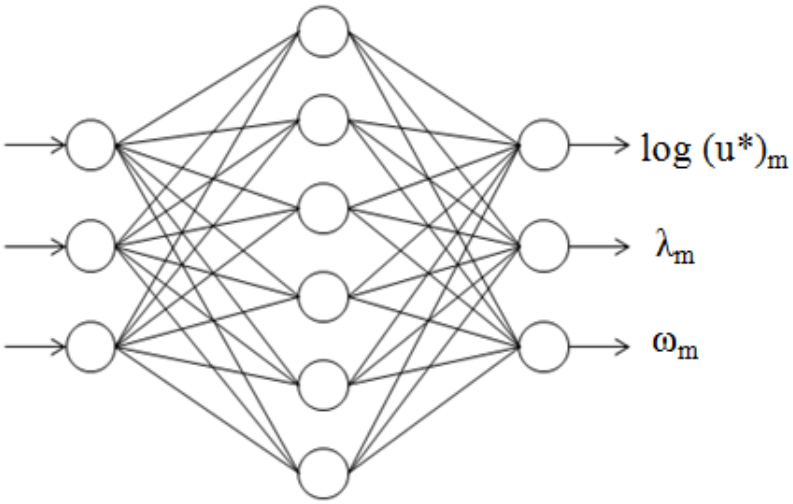


Figure 7

The optimum structure of the trained ANN

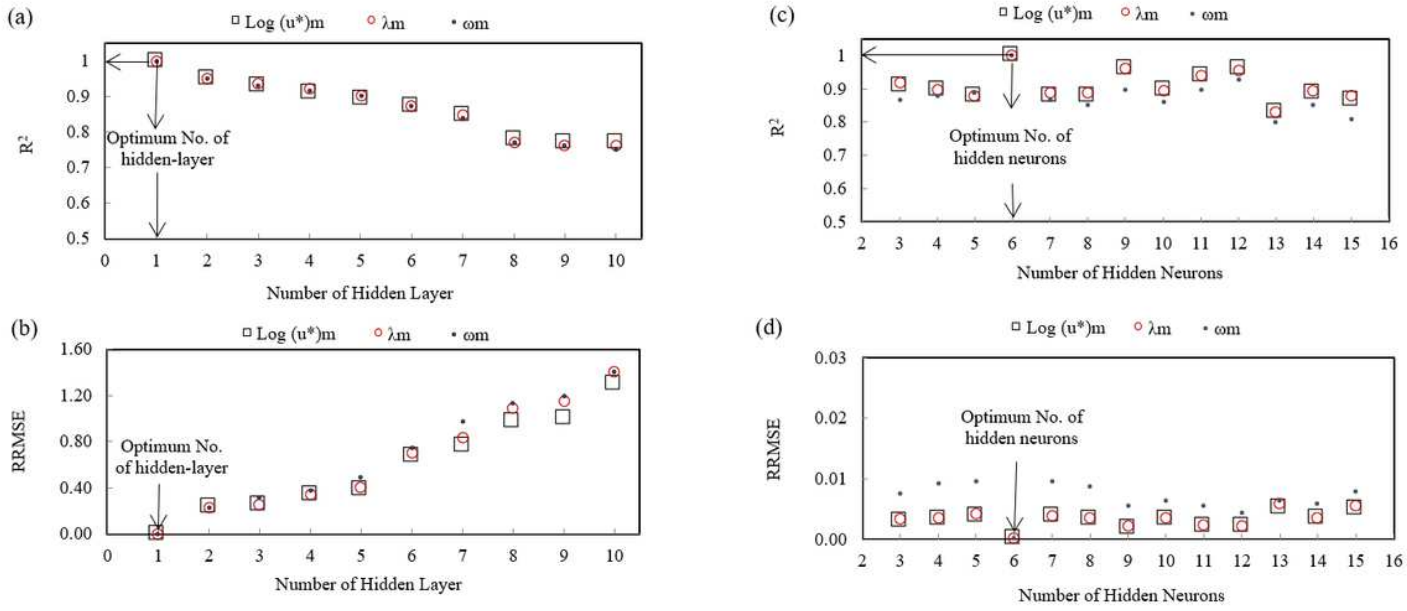


## Figure 8

Sensitivity plots based on number of hidden layer and number of hidden neurons for the developed ANN model structure

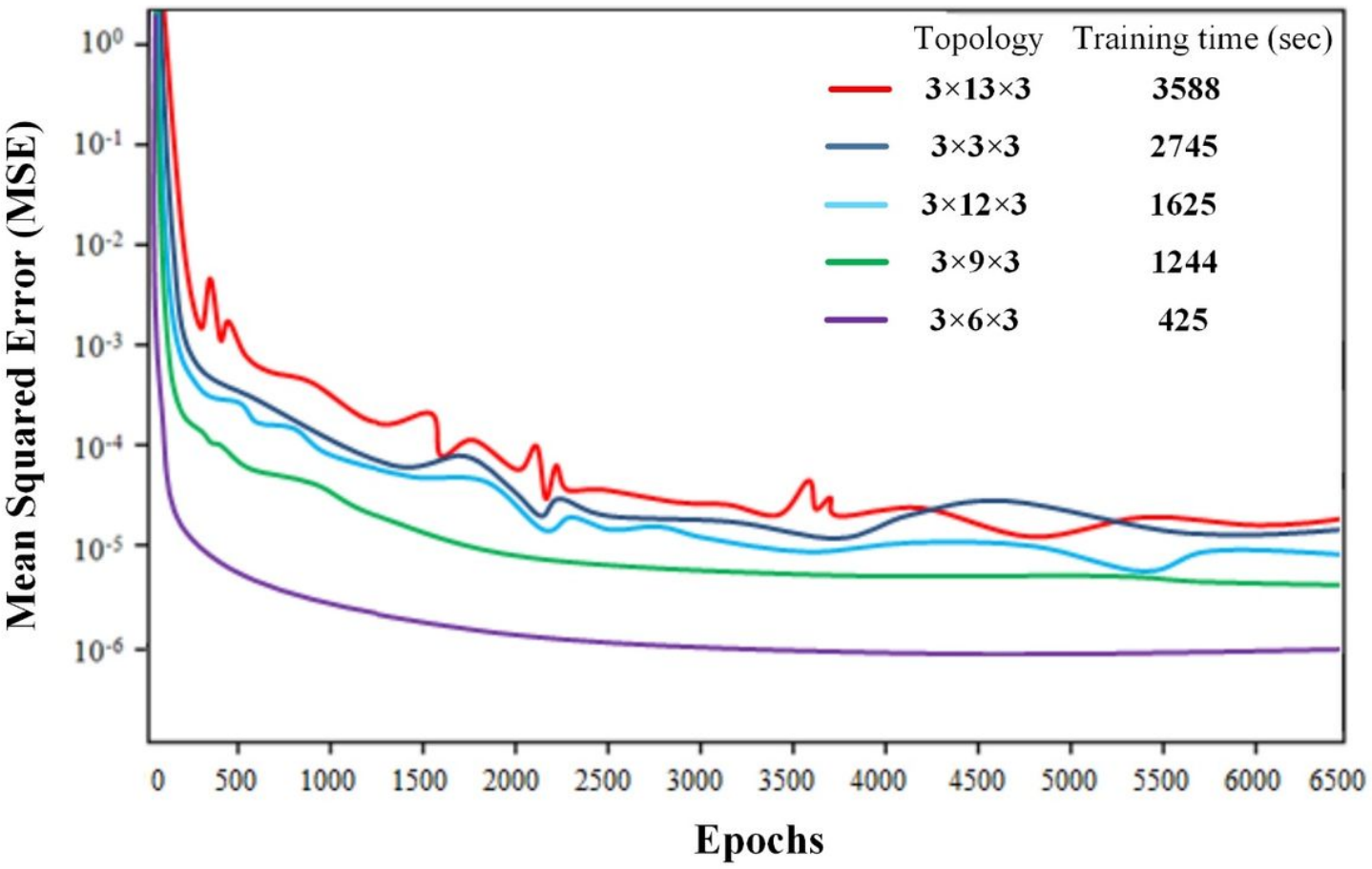


**Figure 9**

Convergence plot of networks with different topology

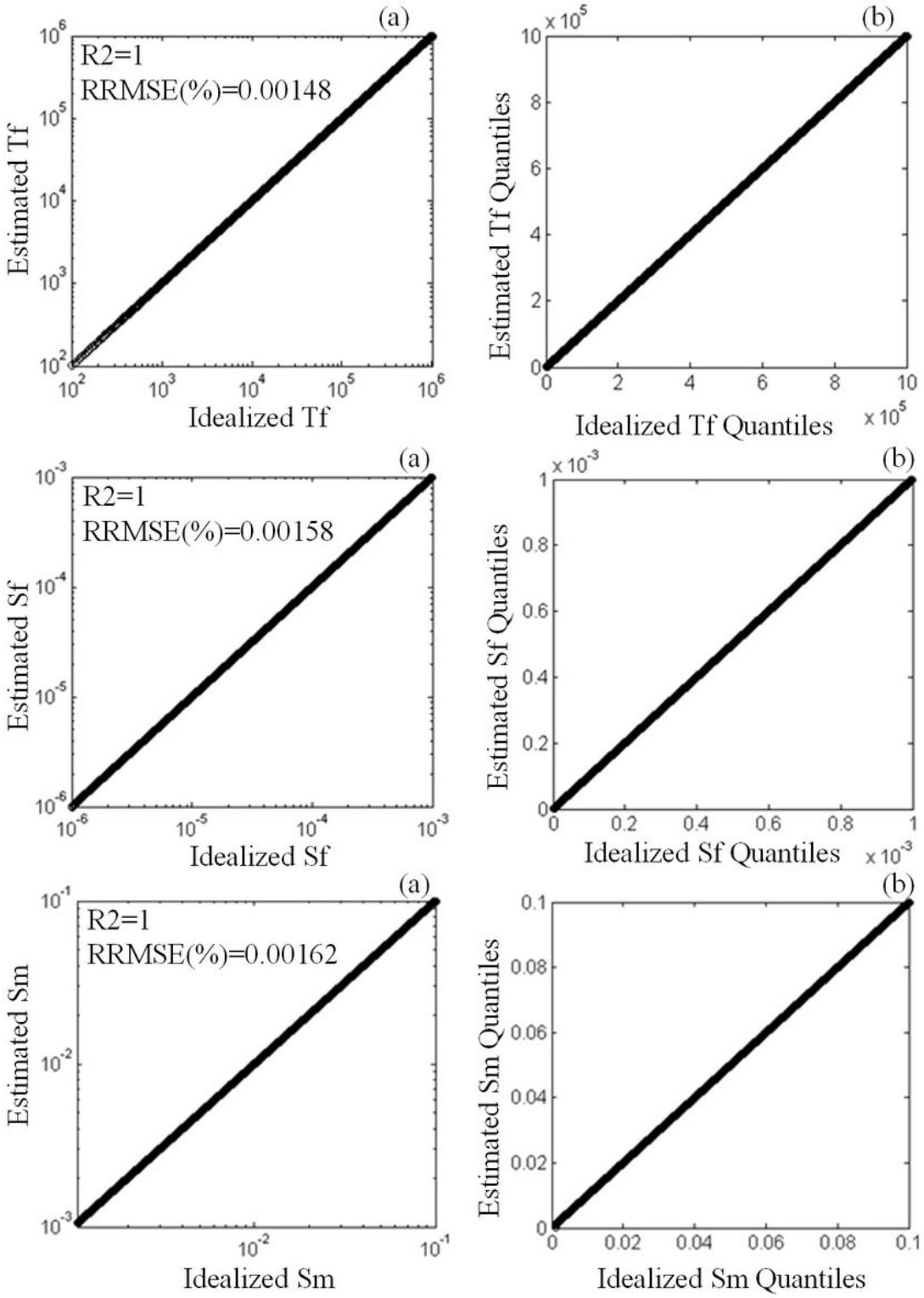


**Figure 10**

a) Idealized versus calculated aquifer parameter values (T_f, S_f, and S_m), b) QQ plot of residuals

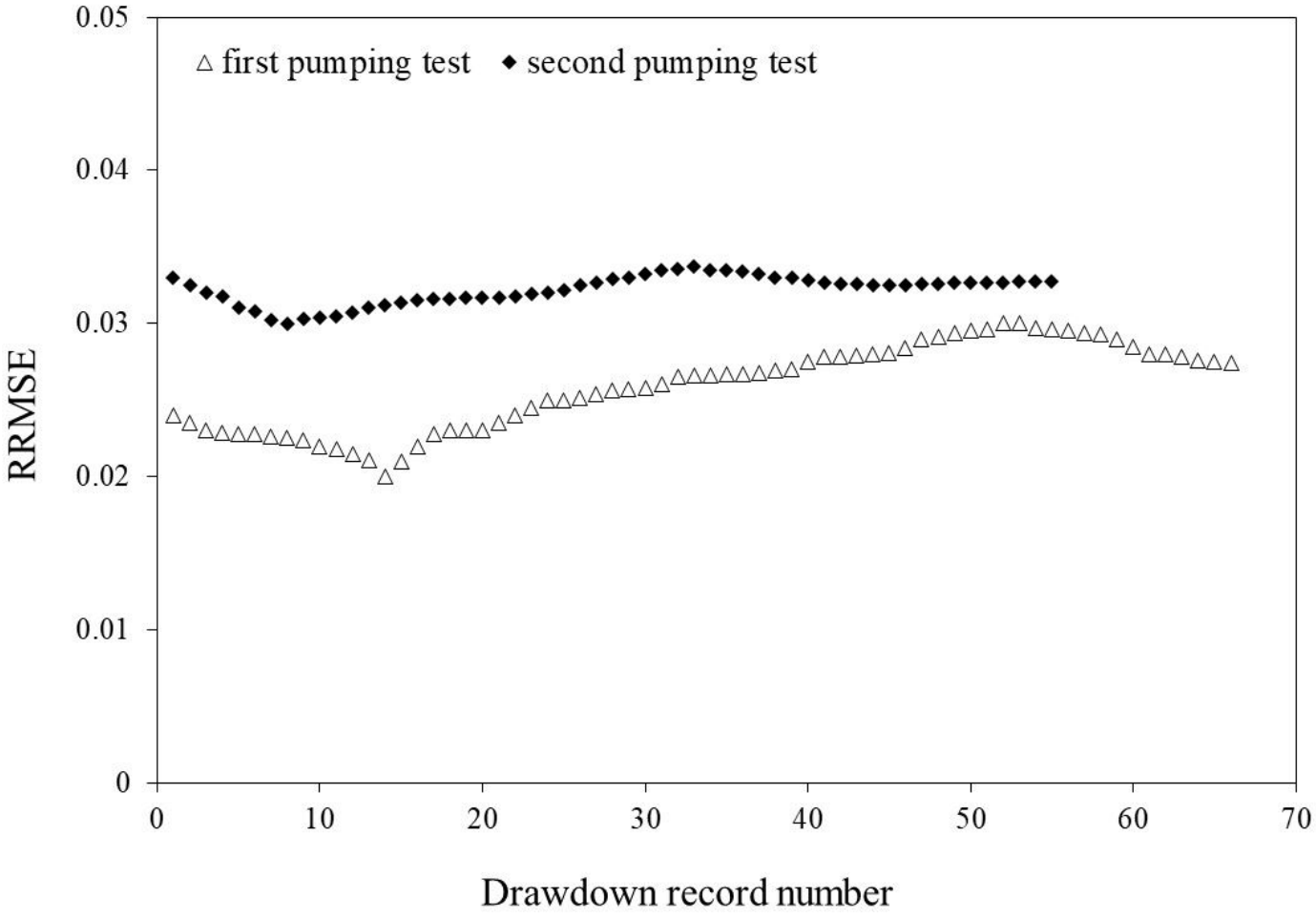


**Figure 11**

RRMSE plot locating the optimum drawdown-time record for the two sets of real pumping test data.

## Supplementary Files

This is a list of supplementary files associated with this preprint. Click to download.

- SupplementaryMaterials1.docx